Article

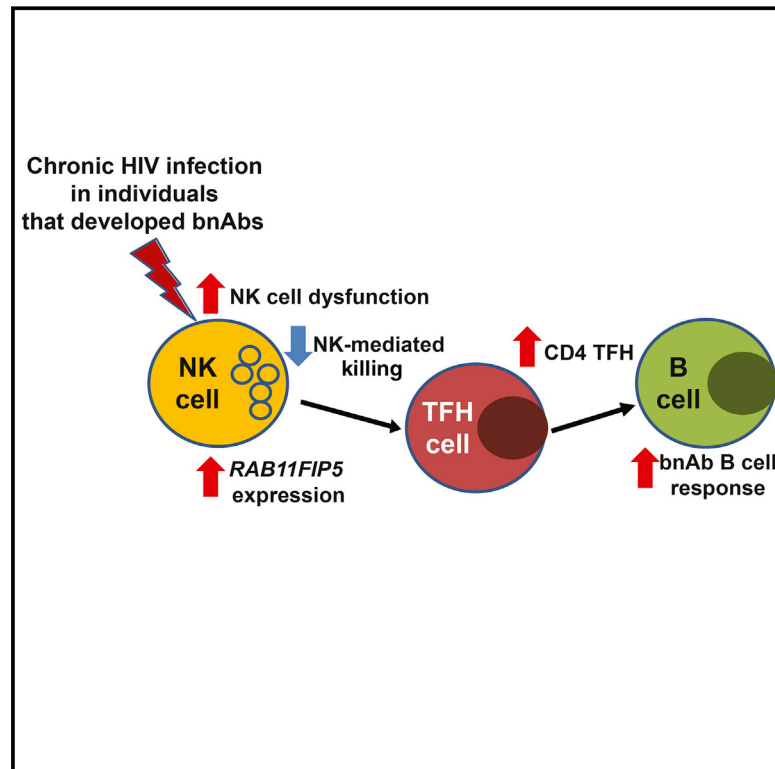# *RAB11FIP5* Expression and Altered Natural Killer Cell Function Are Associated with Induction of HIV Broadly Neutralizing Antibody Responses

## Graphical Abstract

## Authors

Todd Bradley, Dimitra Peppa, Isabela Pedroza-Pacheco, ..., M. Anthony Moody, Persephone Borrow, Barton F. Haynes

## Correspondence

todd.bradley@duke.edu (T.B.), persephone.borrow@ndm.ox.ac.uk (P.B.), barton.haynes@duke.edu (B.F.H.)

## In Brief

Generation of broadly neutralizing antibodies against HIV-1 in humans is linked to the expression of a specific recycling endosome-associated effector in natural killer cells.

## Highlights

- Elevated *RAB11FIP5* expression is associated with HIV-1 bnAb induction

- NK cells show the highest differential *RAB11FIP5* expression

- NK cell subsets are more dysregulated in individuals developing bnAbs

- Rab11Fip5 regulates NK cell function

CellPress

# *RAB11FIP5* Expression and Altered Natural Killer Cell Function Are Associated with Induction of HIV Broadly Neutralizing Antibody Responses

Todd Bradley,[1,2,10,11,*] Dimitra Peppa,[4,10] Isabela Pedroza-Pacheco,[4,10] Dapeng Li,[1,10] Derek W. Cain,[1,2] Ricardo Henao,[3] Vaishnavi Venkat,[3] Bhavna Hora,[1] Yue Chen,[1] Nathan A. Vandergrift,[1,2] R. Glenn Overman,[1] R. Whitney Edwards,[5] Chris W. Woods,[2,3] Georgia D. Tomaras,[1,5,9] Guido Ferrari,[1,5] Geoffrey S. Ginsburg,[2,3] Mark Connors,[6] Myron S. Cohen,[7] M. Anthony Moody,[1,8,9] Persephone Borrow,[4,10,*] and Barton F. Haynes[1,2,9,10,*]

[1]Duke Human Vaccine Institute, Duke University School of Medicine, Durham, NC 27710, USA
[2]Department of Medicine, Duke University School of Medicine, Durham, NC 27710, USA
[3]Center for Applied Genomics and Precision Medicine, Duke University, Durham, NC 27710, USA
[4]Nuffield Department of Clinical Medicine, University of Oxford, Oxford OX3 7FZ, UK
[5]Department of Surgery, Duke University, Durham, NC 27710, USA
[6]Laboratory of Immunoregulation, National Institute of Allergy and Infectious Diseases, National Institutes of Health, Bethesda, MD 20814, USA
[7]University of North Carolina at Chapel Hill, Chapel Hill, NC 27599, USA
[8]Department of Pediatrics, Duke University School of Medicine, Durham, NC 27710, USA
[9]Department of Immunology, Duke University School of Medicine, Durham, NC 27710, USA
[10]These authors contributed equally
[11]Lead Contact
*Correspondence: todd.bradley@duke.edu (T.B.), persephone.borrow@ndm.ox.ac.uk (P.B.), barton.haynes@duke.edu (B.F.H.)
https://doi.org/10.1016/j.cell.2018.08.064

## SUMMARY

HIV-1 broadly neutralizing antibodies (bnAbs) are difficult to induce with vaccines but are generated in ~50% of HIV-1-infected individuals. Understanding the molecular mechanisms of host control of bnAb induction is critical to vaccine design. Here, we performed a transcriptome analysis of blood mononuclear cells from 47 HIV-1-infected individuals who made bnAbs and 46 HIV-1-infected individuals who did not and identified in bnAb individuals upregulation of *RAB11FIP5*, encoding a Rab effector protein associated with recycling endosomes. Natural killer (NK) cells had the highest differential expression of *RAB11FIP5*, which was associated with greater dysregulation of NK cell subsets in bnAb subjects. NK cells from bnAb individuals had a more adaptive/dysfunctional phenotype and exhibited impaired degranulation and cytokine production that correlated with *RAB11FIP5* transcript levels. Moreover, *RAB11FIP5* overexpression modulated the function of NK cells. These data suggest that NK cells and Rab11 recycling endosomal transport are involved in regulation of HIV-1 bnAb development.

## INTRODUCTION

A major goal of HIV-1 vaccine development is to design an immunization strategy that can induce broadly reactive neutralizing antibodies (bnAbs) (Haynes and Burton, 2017; Haynes and Mascola, 2017; Kelsoe and Haynes, 2017; McCoy and Burton, 2017). While HIV-1 infected individuals make bnAbs with a spectrum of activity after years of infection, consistent induction of bnAbs has not been achieved in the setting of vaccination (Bradley et al., 2016; Klasse et al., 2016; Liao et al., 2013; Pauthner et al., 2017; Saunders et al., 2017). One reason bnAbs have not been elicited by vaccination is control of bnAb B cell lineages by immune tolerance (Haynes and Verkoczy, 2014; Kelsoe and Haynes, 2017). Immunologic analyses of HIV-1-infected individuals who make bnAbs compared to those who do not demonstrated those who made bnAbs had higher levels of circulating T follicular helper (Tfh) cells (Locci et al., 2013; Moody et al., 2016), lower levels of T regulatory cells (Tregs) with higher PD-1 expression on Tregs, and a higher frequency of plasma autoantibodies (Moody et al., 2016). This phenotype is similar to the immunologic profile of patients with autoimmune disease and provides support for the hypothesis that HIV-1-infected individuals who make bnAbs have less robust immune control of antibody responses. Thus, precisely defining the cellular and molecular events that lead to the generation of bnAbs during HIV-1 infection is critical for learning how to induce HIV-1 bnAbs.

Antibody responses are controlled not only by CD4^{+} Treg and T follicular regulatory (Tfr) cells, but also by other subsets of immunoregulatory cells (Borrow and Moody, 2017). Notably, natural killer (NK) cells, in addition to their effector role in defense against virus infections and tumors, also have immunoregulatory effects and modulate adaptive immune responses in inflammatory/autoimmune conditions and infections (Gianchecchi et al., 2018; Waggoner et al., 2016). Recent studies in murine models demonstrated a role for NK cells in the control of humoral responses via lysis of CD4 T cells and reduction of CD4 Tfh

availability (Rydyznski et al., 2015; Rydyznski and Waggoner, 2015). NK cell-mediated immunoregulation constrains the generation of autoantibodies in mice chronically infected with murine cytomegalovirus (MCMV) (Schuster et al., 2014), but conversely impairs the induction of neutralizing antibodies in lymphocytic choriomeningitis virus (LCMV)-infected mice (Cook et al., 2015; Rydyznski et al., 2015). Whether NK cells play a similar role in regulating antibody responses in humans remains unclear.

Here, we have performed a transcriptome-wide study in a well-characterized cohort of HIV-1-infected individuals, comparing those who developed plasma bnAb activity with individuals with no plasma bnAb activity (Moody et al., 2016). After controlling for confounding variables, we found Rab11 family-interacting protein 5 (*RAB11FIP5*) transcripts were significantly elevated in subjects who made bnAbs compared to those who did not. The highest differential *RAB11FIP5* expression was in NK cells. *RAB11FIP5* encodes an effector protein in recycling endosomes (Hales et al., 2001; Prekeris et al., 2000), and enhanced expression was associated with changes in NK cell subset distribution and alterations in NK cell functional capacity. These data suggest that NK cell dysregulation and the emergence of an NK cell subset with altered functionality are permissive for bnAb development and implicate Rab11 recycling endosomes as modulators of the HIV-1 neutralizing antibody response.

## RESULTS

### Identification of Differentially Expressed Transcripts in HIV-1-Infected bnAb Individuals

Antibody neutralization breadth was measured in a previously characterized cohort of 239 chronically HIV-infected individuals, from whom a subset of individuals with the highest HIV-1 neutralization breadth were selected as the bnAb group and individuals with low or no neutralization breadth were selected as the control group without bnAbs. RNA-sequencing (RNA-seq) was performed on peripheral blood mononuclear cells (PBMCs) from 47 chronically HIV-1-infected individuals who developed bnAbs (bnAb group, cohort A) and 46 HIV-1-infected individuals who did not have bnAbs (control group, cohort A) (Moody et al., 2016). The 93 HIV-1 infected individuals analyzed consisted of 62 females and 31 males, whose ages ranged from 19–64 years and 84 (88%) were African (Figure S1A).

Transcriptome analysis identified 322 transcripts that were differentially expressed in individuals who developed bnAbs, 222 of which differed by more than 2-fold (Figure 1A; Table S1). Interestingly, 5 of the top 10 most significantly changed genes were involved with endosomal intracellular trafficking pathways (*RAB11FIP5*, *SYT11*, *RAP2A*, *ALS2CL*, and *RABGAP1L*; Figure 1A).

After controlling for age, sex, country, autoantibody status, and viral load, the only gene that remained significantly differentially expressed in the bnAb group was *RAB11FIP5* (Figures 1B and 1C). For the characterization of HIV-1 antibody neutralization breadth in cohort A, we previously used a neutralization panel of 12 HIV-1 isolates and performed a principal component analysis of the data. Principal component 1 (PC1) scores are a proxy for neutralization breadth accounting for neutralization magnitude; a higher PC1 score indicates more neutralization breadth and a lower PC1 score means less breadth (Moody et al., 2016). Expression levels of *RAB11FIP5* correlated with neutralization breadth ($r = 0.50$, $p \leq 0.05$; Spearman, Figure 1D) but not with viral load ($r = 0.09$, NS; Spearman, Figure 1E). qPCR of PBMCs from bnAb individuals analyzed by RNA-seq (cohort A) combined with a second smaller cohort of HIV-1 infected individuals from the United States composed of individuals who produced bnAbs and those who had lower levels of plasma neutralizing antibodies (cohort B, n = 21) (Moody et al., 2016) confirmed the higher level of *RAB11FIP5* expression in PBMCs of those that made bnAbs (Figure S1B).

### NK Cells from bnAb Individuals Have Upregulated *RAB11FIP5* and Transcriptional Signatures of Increased Peripheral Maturation with Altered Functionality

PBMC from bnAb or control individuals with the highest and lowest PBMC *RAB11FIP5* expression levels, respectively, were separated into CD19 B cells, CD4 T cells, CD8 T cells, and non-B/T cells (Figure S1C), and the level of expression of *RAB11FIP5* in each subset was determined by qPCR. There were no significant differences in viral load in the two groups of selected individuals. The highest difference in expression of *RAB11FIP5* between subjects with and without bnAbs was in CD8 and non-B/T cells (Figure 1F). Non-B/T cells were further fractionated into CD14+ monocytes, CD56+CD16+ NK cells, and plasmacytoid (p) and myeloid (m) dendritic cell (DC) populations (Figure S1D), and the highest differential expression of *RAB11FIP5* was found to be in the NK cell subset (Figure 1G). RNA-seq performed on NK cells from bnAb and no-bnAb control individuals also detected the highest differential expression of *RAB11FIP5* mRNA within the NK cell population (Figure S1E; p = 0.03, Wilcoxon-Mann-Whitney). Thus, we hypothesized that alterations in the NK cell compartment may contribute to the development of bnAbs during HIV-1 infection.

Transcriptome analysis of the purified CD3−CD56+CD16+ NK cells from bnAb and control individuals by RNA-seq identified 95 transcripts (44 upregulated and 51 downregulated) that were differentially expressed in individuals from the bnAb group versus control subjects without bnAbs, one of which was *RAB11FIP5* (Figure S2A; Table S2). We did not control for viral load in this analysis due to the small sample size. We found that NK cells from bnAb and control subjects expressed equivalent levels of *GZMB*, *GZMH*, *GZMM*, and *PRF1* (perforin) killing molecules, but NK cells from bnAb subjects had lower expression of *GZMA* and *GZMK*, that mediate caspase-independent cell lysis and also lower expression of *TNFSF10* (TRAIL) that mediates caspase-dependent cell lysis (Figure S2B). NK cells from bnAb individuals also expressed lower levels of *PLZF*, interleukin (IL)12 and IL18 receptor transcripts and *CD27* while having increased *CD6* expression (Figure S2C). These results indicated that CD3−CD56+CD16+ NK cells, the majority of which are mature CD56dim NK cells, had transcripts indicative of acquisition of an adaptive-like NK cell phenotype (Béziat et al., 2010; Hayakawa and Smyth, 2006; Schlums et al., 2015; Takeda et al., 2005) and may have altered NK function in the bnAb group.
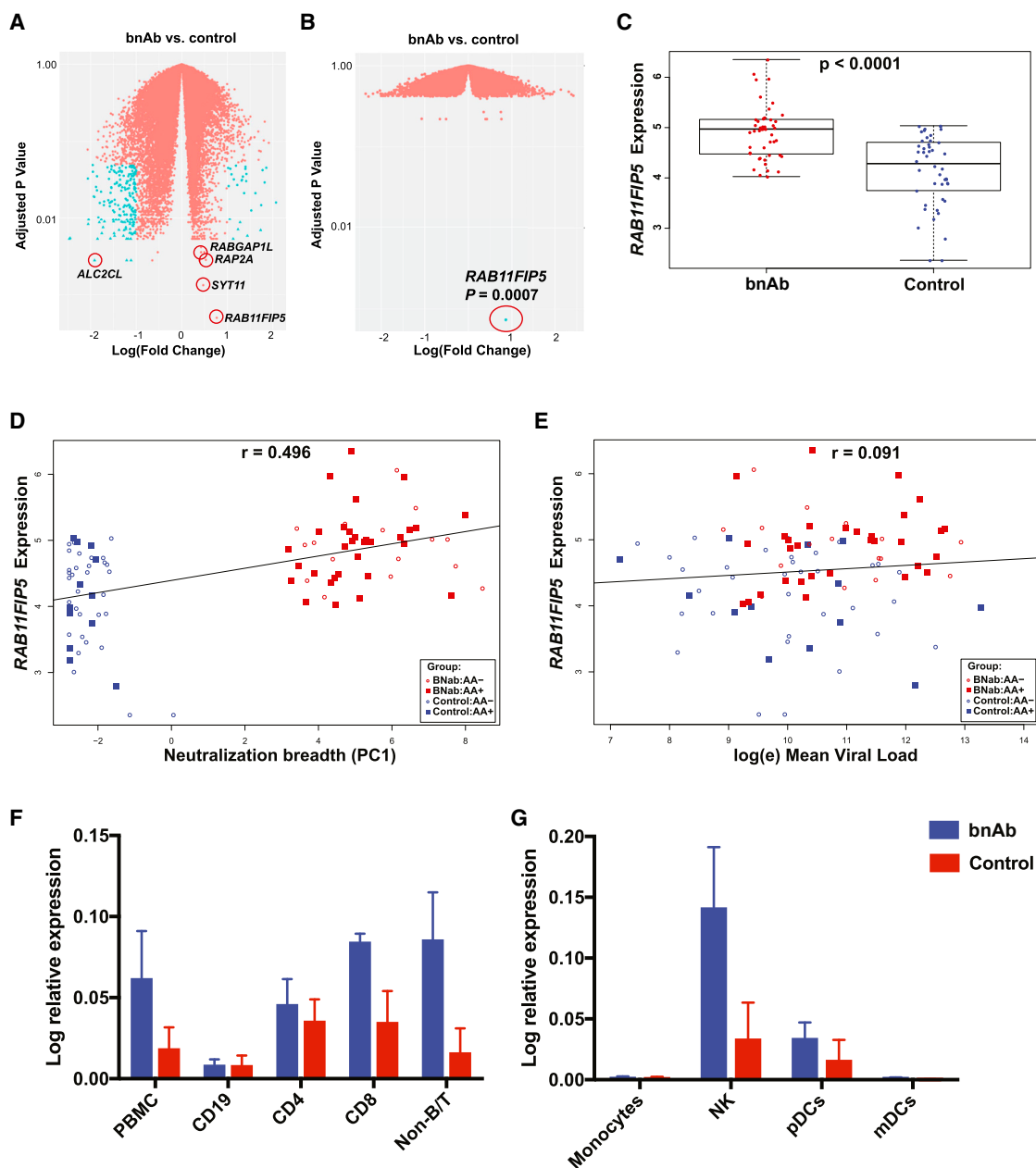
**Figure 1. Upregulation of *RAB11FIP5* in bnAb Individuals**

(A and B) Plots of differential transcript expression in the bnAb group compared with control group (A) and after controlling for age, sex, country, autoantibody status, and viral load (B). Transcripts with p < 0.05 and log (FC) >1 are colored in blue. Transcripts associated with vesicle trafficking are circled.

(C) Boxplot of *RAB11FIP5* expression levels for each individual in the bnAb (n = 47) and control group (n = 46; t test).

(D and E) Spearman correlations of *RAB11FIP5* expression (y axis) and neutralization breadth (principal component 1) (D) or viral load (E). bnAb group are in red and control group in blue; solid fill autoantibody positive and open fill autoantibody negative individuals.

(F and G) Bar graphs of quantitative PCR of *RAB11FIP5* of PBMC, CD19+, CD4+, CD8+ and non-B/T cells (F) and monocytes, NK, pDC and mDC cells (G). BnAb group (n = 3 or 4) shown in blue and control group (n = 3 or 4) shown in red. The groups of HIV-1 infected bnAb and control subjects selected for this analysis were matched for viral load. Group average and SEM shown.

See also Figures S1 and S2 and Table S1.

## NK Cell Subset Redistribution in bnAb Individuals

In humans, NK cells are classically grouped into two main subsets on the basis of expression of CD56 and CD16. The CD56brightCD16$^{-/+}$ subset is primarily specialized for cytokine production whereas the CD56dimCD16$^{+}$ NK cells represent a more mature subset, exhibiting high levels of perforin and enhanced killing. Chronic infection with viruses including HIV-1 is associated with a significant redistribution of the NK
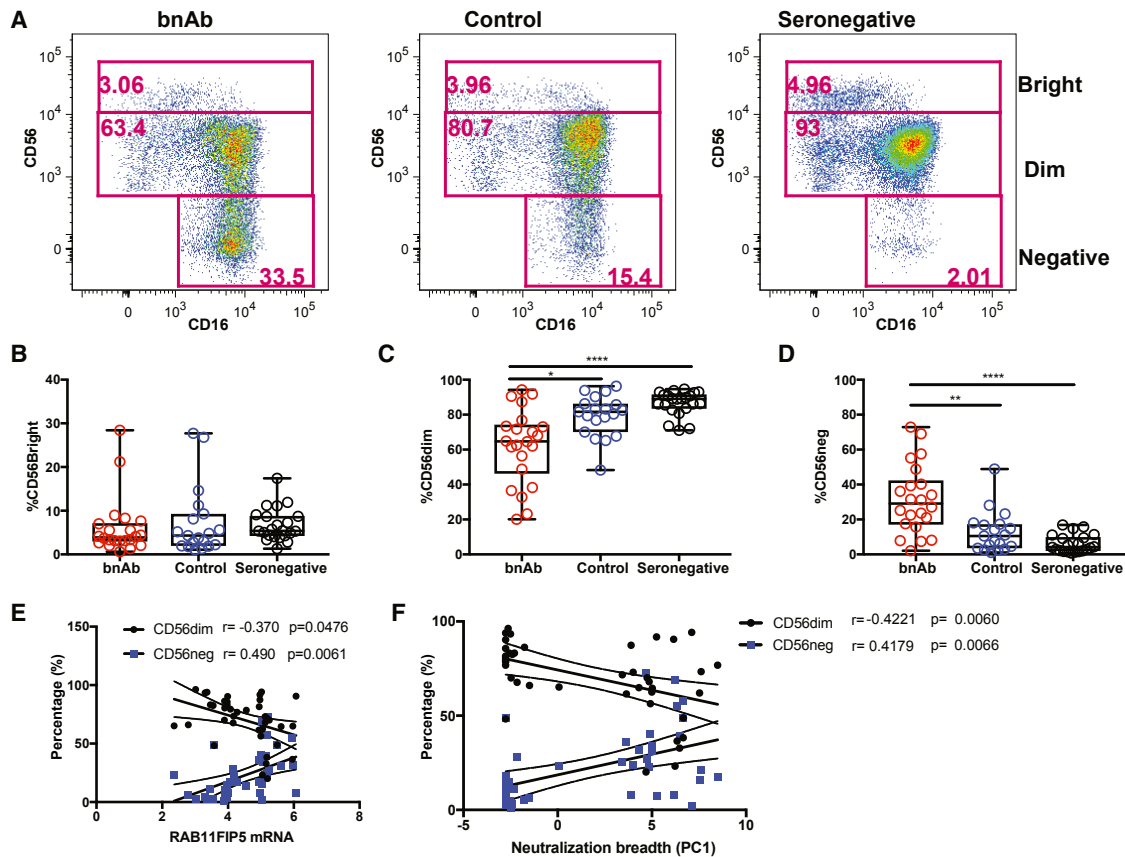
**Figure 2. More Pronounced NK Cell Subset Redistribution in bnAb versus Control Subjects**

(A) Representative pseudocolor flow cytometry plots from bnAb, control, and HIV-seronegative individuals showing NK cell subsets distinguished on the basis of CD56 and CD16 expression. Gated on live, CD19⁻CD14⁻CD4⁻CD3⁻ lymphocytes.

(B–D) Boxplots of the percentage of NK cells that were CD56bright (B), CD56dim (C), and CD56⁻CD16⁺ (CD56neg) (D) in individuals in the bnAb (red; n = 22), control (blue; n = 19), and HIV-seronegative (black; n = 19) groups. Each symbol represents data from an individual subject and the box-and-whisker plots show the median, quartiles, and range. *p < 0.05, **p < 0.01, ***p < 0.001, ****p < 0.0001. p values are corrected for multiple comparisons analysis and viral load.

(E and F) Spearman correlations of (E) *RAB11FIP5* mRNA levels in total PBMC and (F) plasma HIV-1 neutralization breadth (PC1) with the percentage of CD56dim (black) and CD56⁻CD16⁺ (blue) NK subsets within total NK cells.
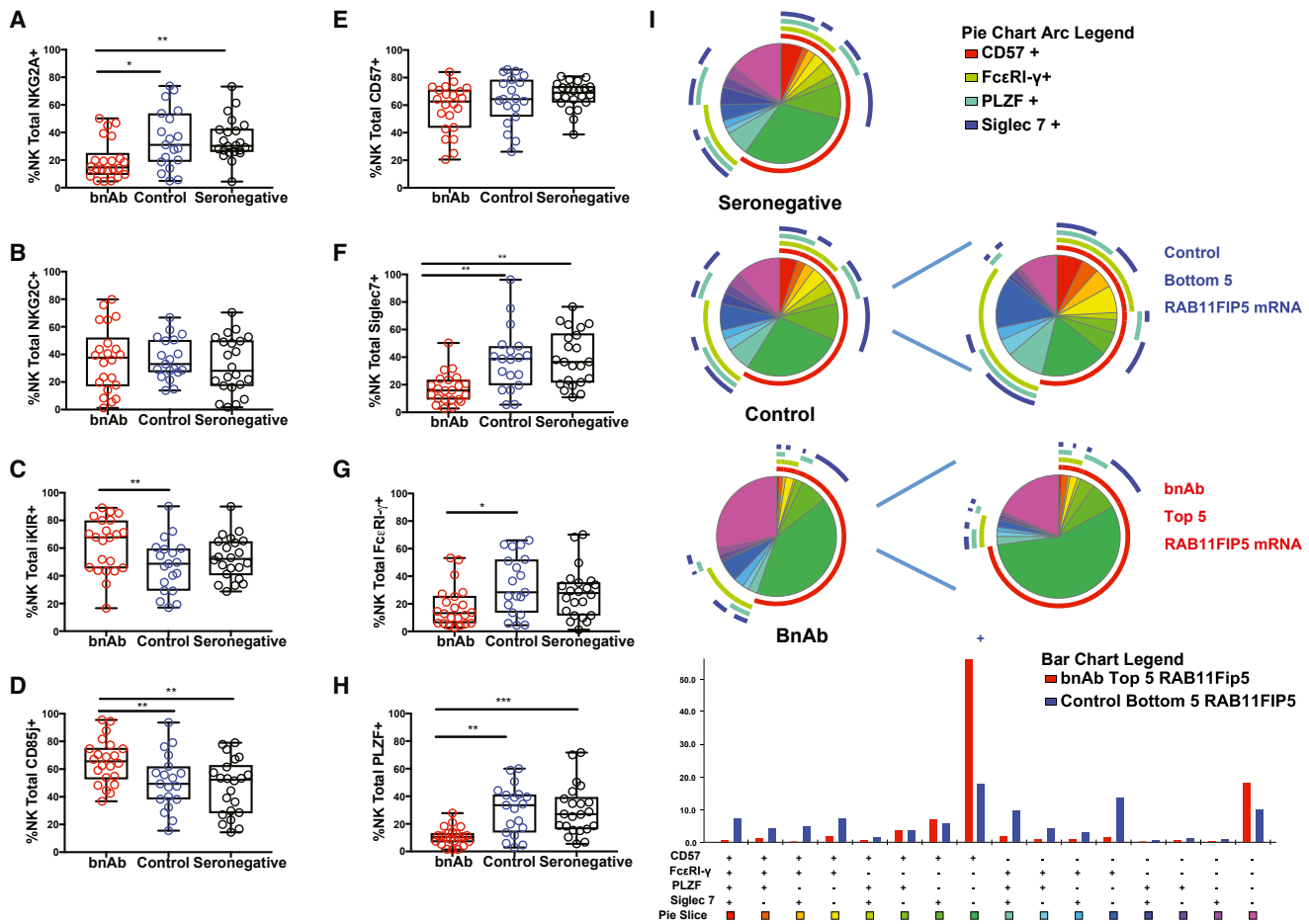
See also Figure S3 and Table S2.

compartment, with the emergence of a third aberrant and anergic CD56⁻CD16⁺ NK cell subset (Alter et al., 2005; Fauci et al., 2005; Mavilio et al., 2003). NK cell subset distributions were determined in PBMCs from individuals in the bnAb (n = 22) and control (n = 19) groups and a demographically matched HIV seronegative (n = 22) group (Figure S3A). We selected the top 10 *RAB11FIP5*-expressing individuals in the bnAb group and the lowest 10 *RAB11FIP5*-expressing individuals in the control group, with all other individuals being selected to ensure matching between groups for age, sex, and country of origin. No differences were observed between groups in the percentage of total NK cells within live lymphocytes (Figure S3B). The proportion of CD56brightCD16⁺/⁻ NK cells also did not differ significantly between any of the groups (Figures 2A and 2B). However, in the bnAb individuals, the CD56dim subset was significantly decreased compared to HIV-1 control and HIV-1 seronegative subjects (Figures 2A and 2C). Notably, in bnAb individuals, a high proportion of NK cells had a CD56⁻CD16⁺ phenotype (mean = 31.5 ± 4.2 and ranging up to 72.9% of total NK

cells), whereas CD56⁻CD16⁺ cells comprised a smaller proportion of total NK cells in control individuals (mean = 12.6 ± 2.7) and a minor subset of NK cells in HIV-1 seronegative subjects (mean = 6.2 ± 1.1) (Figures 2D and S3C).

The proportion of CD56dim cytotoxic NK cells correlated negatively with *RAB11FIP5* mRNA (Figure 2E) and HIV-1 antibody neutralization breadth (PC1 scores) (Figure 2F), whereas a positive correlation was observed between the CD56⁻CD16⁺ subset and *RAB11FIP5* mRNA expression levels in PBMC (Figure 2E) and PC1 scores (Figure 2F). These data demonstrated that NK cell subset redistribution and the emergence of an aberrant NK cell population were associated with both PBMC *RAB11FIP5* expression and plasma HIV-1 neutralization breadth.

## NK Cells Had an Adaptive-like Signature in bnAb Individuals

Individuals with bnAbs had a lower proportion of total NK cells expressing the inhibitory receptor NKG2A (Figure 3A),

**Figure 3. Increased Frequencies of Mature and Adaptive-like NK Cells in bnAb Subjects**

(A–H) Boxplots of the percentage of total NK cells expressing NKG2A (A), NKG2C (B), iKIR (cocktail of antibodies against KIR2DL1/S5, KIR2DL2/L3/S2, KIR3DL2, KIR3DL1) (C), CD85j (D), CD57 (E), Siglec7 (F), FcεRI-γ (G), and PLZF (H) in bnAb (red; n = 22), control (blue; n = 19) and HIV seronegative individuals (black; n = 22). Each symbol represents data from an individual subject and the box-and-whisker plots show the median, quartiles, and range. *p < 0.05, **p < 0.01, ***p < 0.001. p values are corrected for multiple comparisons analysis and viral load.

(I) SPICE (simplified presentation of incredibly complex evaluations) analysis of CD57, FcεRI-γ, PLZF, and Siglec7 receptor combinations on total NK cells in HIV seronegative individuals (n = 22), control (n = 19) and bnAb (n = 22) subjects. SPICE pie charts are shown for seronegative, control and bnAb groups and for individuals with the lowest *RAB11FIP5* mRNA (bottom 5; blue; n = 5) in the control group and highest levels of expression of *RAB11FIP5* mRNA in total PBMC (top 5; red; n = 5) in the bnAb group. SPICE bar charts depict the proportion of total NK cells expressing the indicated receptor combinations in the top 5 *RAB11FIP5* subjects in the bnAb group (red bars) and bottom 5 *RAB11FIP5* subjects in the control group (blue bars). Student's t test was used to compare samples in SPICE. + p < 0.0001.

See also Figures S4 and S5.

but no difference in the proportion positive for the activating receptor NKG2C (Figure 3B). The proportion of total NK cells positive for inhibitory KIRs (identified using a cocktail of antibodies against KIR2DL1, KIR2DL2/L3/S2, KIR3DL1, KIR3DL2) was higher in bnAb subjects compared to HIV-1 controls (Figure 3C), and the proportion of cells positive for the inhibitory receptor CD85j was higher in bnAb subjects compared to both HIV-1 control and in HIV-1 seronegative individuals (Figure 3D). Lower frequencies of NKG2A expressing NK cells coupled with increased frequencies of cells expressing inhibitory NK receptors suggested an accentuated shift toward NK cell maturation in the bnAb group. However, the proportion of cells positive for CD57, also a marker

of terminal NK cell differentiation, did not differ among the 3 groups (Figure 3E).

Adaptive NK cells have been shown to have decreased expression of the inhibitory receptor Siglec7, the signaling molecule FcεRIγ and the transcription factor promyelocytic leukemia zinc finger (PLZF) (Della Chiesa et al., 2016; Schlums et al., 2015). The NK cells from individuals in the bnAb group had significantly lower proportions of Siglec7 and PLZF-expressing cells compared to the control and seronegative groups and a lower proportion of NK cells expressed FcεRγ compared to the control group (Figures 3F–3H). Co-expression analysis using Boolean gating revealed an enrichment of CD57+ FcεRIγ− PLZF− Siglec7− NK cells within the bnAb

group, particularly in subjects with high *RAB11FIP5* mRNA levels compared to HIV-1 control individuals with low *RAB11FIP5* mRNA levels (Figure 3I).

Subset analysis of NK cell populations revealed similar differences between groups in receptor expression on both the CD56dim and CD56⁻CD16⁺ NK cell subsets (Figures S4A and S4B). Notably the CD56⁻CD16⁺ subset, which was more predominant in the bnAb group, had the lowest frequency of cells positive for Siglec-7, FcεRIγ, and PLZF expression (Figures S4A and S4B) suggesting that this subset shares features of adaptive NK cells. Significant correlations were observed between *RAB11FIP5* transcript levels in PBMC and mature/adaptive-like NK cell attributes and additional features signifying their aberrant dysregulation: a negative correlation with NKG2A (r = −0.59, p = 0.001; Spearman), positive correlations with levels of expression of CD85j (r = 0.53, p = 0.003; Spearman) and inhibitory KIRs (r = 0.58, p = 0.001; Spearman), and negative correlations with Siglec7 expression (r = −0.50, p = 0.005; Spearman), FcεRIγ (r = −0.62, p = 0.0006; Spearman), and PLZF (r = −0.60, p = 0.001; Spearman) (Figures S5A–S5F). These data suggested a preferential enrichment of terminally differentiated adaptive-like NK cells in individuals who develop bnAbs.

Adaptive-like NK cells have also been described in individuals infected with human cytomegalovirus (HCMV) that have altered functionality (Foley et al., 2012; Lopez-Vergès et al., 2011; Schlums et al., 2015). We determined that all the individuals in the bnAb group, and all but one individual in the control group, had positive serum antibodies against HCMV and found no significant differences in HCMV antibody titers between the bnAb and control groups (Figure S5G).

### Altered NK Cell Functions in bnAb Individuals

Following stimulation with MHC class I-low target cells (.221 cell line) the proportion of NK cells expressing CD107a, a marker of degranulation, was lower in the bnAb group compared to control and HIV-1 seronegative groups (Figures 4A and 4B). The proportion of cells expressing interferon (IFN)-γ was lower in the bnAb group than the seronegative group, and a similar pattern was observed comparing bnAb and control HIV-1 groups although this did not reach statistical significance (Figures 4A and 4B). The proportion of NK cells producing tumor necrosis factor alpha (TNF-α) was also lower in individuals who developed bnAbs compared to both control and HIV-1 seronegative subjects (Figures 4A and 4B). *RAB11FIP5* transcript levels in PBMC were negatively correlated with NK cell function (Figure 4C). Moreover, we found that NK cell function inversely correlated with plasma neutralization breadth (PC1 scores; r = −0.4077, p = 0.01; Spearman; Figure S6A).

Subset analysis of NK cells showed a similar reduction in the proportion of cells with degranulation potential and cytokine production in the CD56dim subset in the bnAb group compared to seronegative subjects (Figure S6B), while the CD56⁻CD16⁺ subset had a reduced frequency of cells with degranulation potential and cytokine production in all groups (Figure S6C). Thus, the over-representation of the CD56⁻CD16⁺ NK cell population in the bnAb group contributed to the impairment in bnAb group NK cell function.

### NK Cells Reduce Tfh Availability for Interaction with B Cells

Determining if human NK cells are capable of controlling humoral responses by regulating Tfh availability in a manner analogous to observations in mice has not been demonstrated. To investigate this, an *in vitro* NK/Tfh/B co-culture system was used (Figures 5A and S6D). Activated NK cells induced a significant reduction in both CD4 Tfh number and proliferation in this Tfh/B co-culture system (Figures 5A–5C). We did not observe a similar effect on CD4 Tfh cells when resting NK cells were used (data not shown). We found that there was also a reduction in the number of class-switched memory B cells and number of plasmablasts in Tfh/B cell co-cultures performed in the presence of activated NK cells (Figures 5D and 5E). Moreover, production of IgM isotype antibodies was significantly reduced, with a trend for a reduction in IgG antibodies, when NK cells were added to the co-culture (Figures 5F and 5G). These results indicated the capacity for NK cells to regulate CD4 Tfh availability and reduce B cell class switching, differentiation into plasmablasts and antibody production during humoral responses in humans and suggest that impairments in NK cell functionality such as those observed in HIV-1-infected individuals generating bnAbs may lead to increased CD4 Tfh numbers, facilitating bnAb induction.

### Single-Cell RNA-Seq Characterization of *RAB11FIP5* Expression in NK Cell Subsets

To investigate the relationship between *RAB11FIP5* expression and NK cell dysregulation, NK cells from a single chronically HIV-infected donor who developed bnAbs were sorted into 3 populations (CD56bright, CD56dim, or CD56⁻) and subjected to single-cell RNA-seq (Figure S3A). Transcriptome information from 22,242 single NK cells was clustered and the dimensionality was reduced and visualized by t-distributed stochastic neighbor embedding (tSNE) (Satija et al., 2015). The numbers of unique molecular identifiers (average = 4,008 ± 999.6) and genes detected per cell (average = 1,387 ± 220.6) in all three libraries were similar and normalized to the library with the lowest values (Figure S7A). The three NK populations formed distinct clusters, indicating unique transcriptome programs for each NK cell subset (Figure 6A). Additional subclusters were identified within each sample that may represent individual cells transitioning between states or transcriptionally distinct NK cell subclusters not defined by CD56 surface marker expression. Individual cells that expressed the highest levels of *RAB11FIP5* mRNA were most frequent in the CD56⁻ dysfunctional NK cell subset in this individual, although some cells with *RAB11FIP5* transcript expression were identified in the other subsets. (Figures 6B and 6C). We next determined differentially expressed transcripts in NK cells that expressed *RAB11FIP5* compared to NK cells that expressed undetectable levels of *RAB11FIP5*, using a likelihood ratio based on zero-inflated data test for single cell gene expression (McDavid et al., 2013). Seven transcripts were significantly upregulated in *RAB11FIP5*-expressing NK cells compared to *RAB11FIP5* negative NK cells and 18 transcripts downregulated (Figure 6D; Table S3). The 7 upregulated transcripts were all associated with NK cell activation and function. Upregulation of *CCL5*, *LGALS1*, *GZMH*, *CD3E*, and *KLRG1* was observed in *RAB11FIP5* cells in all three NK cell subsets; whereas *CCL3L3*
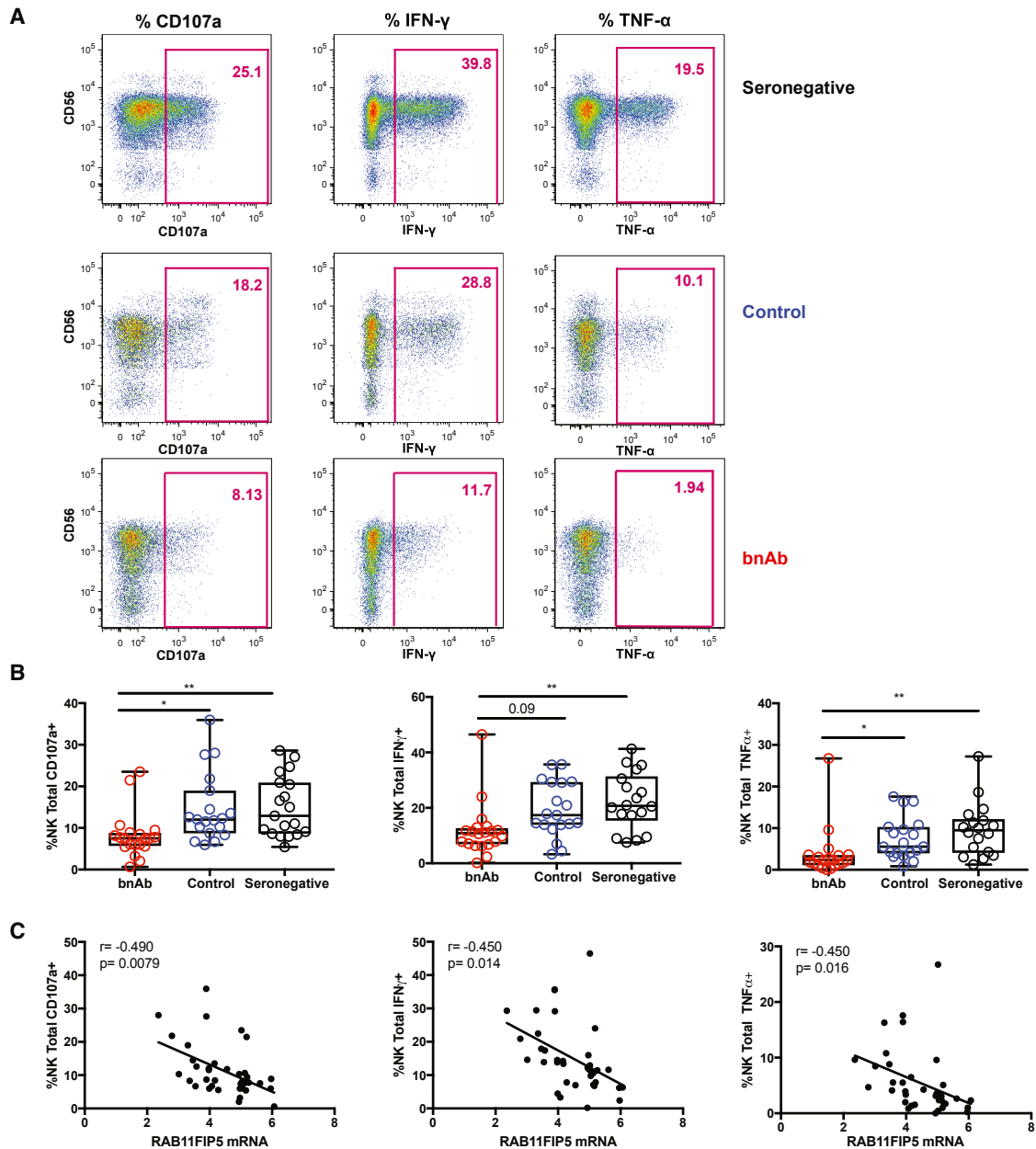
**Figure 4. Decreased Function of NK Cells in bnAb Subjects**

(A and B) Representative pseudocolor flow cytometry plots from individual seronegative, control, and bnAb groups (A) and summary boxplots for all individuals analyzed in each group (B) showing CD107a expression, IFN-γ production, and TNF-α production by total NK cells following stimulation with MHC class I low target cells. Each symbol represents data from an individual subject and the box-and-whisker plots show the median, quartiles, and range. *p < 0.05, **p < 0.01. p values are corrected for multiple comparisons analysis and viral load (bnAb, n = 20; control, n = 19; seronegative, n = 18 or 19).

(C) Spearman correlation of *RAB11FIP5* mRNA levels in total PBMC with percentage of total NK cells expressing CD107a, producing IFN-γ, and producing TNF-α in response to target cell stimulation.

See also Figure S6.

and *IFNG* were only upregulated within the more mature CD56dim and CD56⁻ NK cell populations (Figure S7B). The frequency of IFNγ producing cells was lower in .221 cell-stimulated total NK cells and in the CD56⁻ NK subset (Figures 4B and S6); however, in unstimulated bnAb NK cells, *IFNG* transcript expres-

sion was highest in the CD56⁻ subset both in individual cells studied by single cell RNA sequencing (scRNA-seq) and in bulk NK sub-populations analyzed by RNA-seq from HIV-infected individuals who developed bnAbs (Figure S7C). Mature NK cells have an epigenetically more accessible IFNγ locus
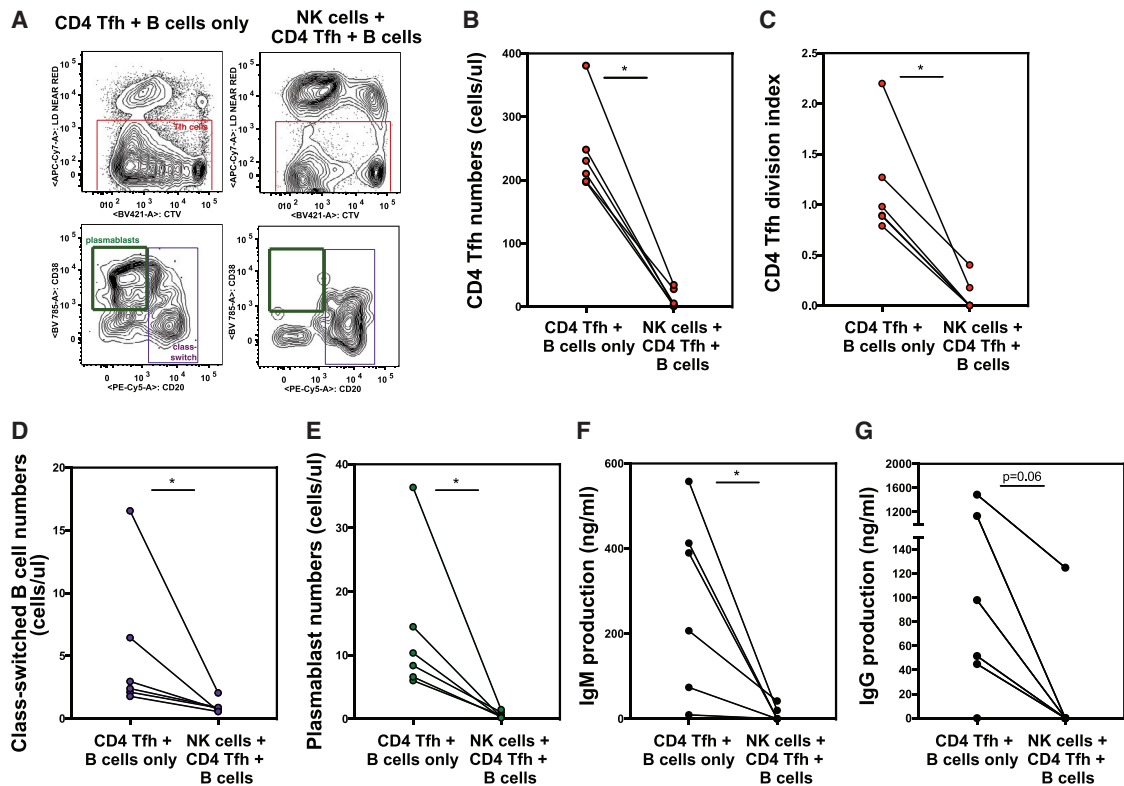
**Figure 5. NK Cells Reduce Tfh Numbers and Help for B Cells in an *In Vitro* Tfh-B Cell Co-culture System**

Total NK cells and resting CD127hiCD25lowCXCR5+CD4+Tfh cells isolated from the peripheral blood of HIV seronegative donors (n = 6) were activated with IL-2/12/15/18 (NK cells) or SEB (Tfh) then mixed and co-cultured with autologous naive B cells at a B:Tfh:NK ratio of 2:1:5 in the presence of SEB.

(A) Representative example of live Tfh cells (gated within CD3+CD4+CD19−CD56− cells), class-switched B cells and plasmablasts (both gated within live CD3−CD4−CD19+IgM−IgD− cells) in the presence or absence of NK cells measured 6 days later.

(B and C) CD4 Tfh numbers (B) and division index (C).

(D and E) Numbers of class-switched memory B cells (D) and plasmablasts (E).

(F and G) Supernatant levels of total IgM (F) IgG (G). Paired data from Tfh-B cell co-cultures carried out in the presence and absence of NK cells with samples from individual donors are shown. *p < 0.05. Wilcoxon matched-pairs signed rank test; p values corrected for multiple comparison analysis.

See also Figure S6.

than immature NK cells and can constitutively express IFNγ transcript (Mah and Cooper, 2016). Thus, these data demonstrated that *RAB11FIP5* transcript expression was most frequent in CD56− NK cells in a single HIV-infected donor who developed bnAbs, and *RAB11FIP5*-expressing cells exhibited upregulation of transcripts associated with NK cell maturation/homeostasis and altered functionality.

### Overexpression of Rab11Fip5 Increased Cytokine Release and Degranulation in NK-92 Cells

The observation that NK cells with upregulated *RAB11FIP5* transcript also had upregulated *IFNG* transcripts suggested that upregulation of *RAB11FIP5* by adaptive/dysregulated NK cells could be a mechanism to restore NK cell function rather than suppress NK cell function. To study this issue, we transduced the NK effector cell line, NK-92, with an expression vector that encoded Rab11Fip5 or a control vector (zsGreen). We stimulated the Rab11Fip5-expressing NK-92 cells and the control transduced cells with PMA and ionomycin and determined intracellular expression of IFNγ and sur-

face expression of CD107a (Figure 7A). NK-92 cells that overexpressed Rab11Fip5 had increased IFNγ and CD107a expression after stimulation compared with control cells (Figure 7A). Stimulated Rab11Fip5-expressing NK-92 cells also had increased secretion of IFNγ into cell culture supernatants (Figure S7D). NK-92 cells transduced with Rab11Fip5 co-cultured with K562 target cells also exhibited increased granzyme B activity compared to control transduced cells, as a surrogate of NK mediated killing. This increase was observed at all effector to target ratios with K562 cells in three independent experiments (Figures 7B and S7E). Western blot analysis demonstrated high expression of Rab11Fip5 in the transduced cells, while non-transduced NK-92 cells expressed very low levels of Rab11Fip5 (Figure 7C). Stimulation of Rab11Fip5-transduced NK-92 cells with K562 target cells demonstrated upregulation of expression of Rab11Fip5 after 10 hr of NK cell:target cell co-culture (Figure 7C). These data suggested that upregulation of Rab11Fip5 can occur as a consequence of NK cell activation via receptor interaction with ligands on target cells.
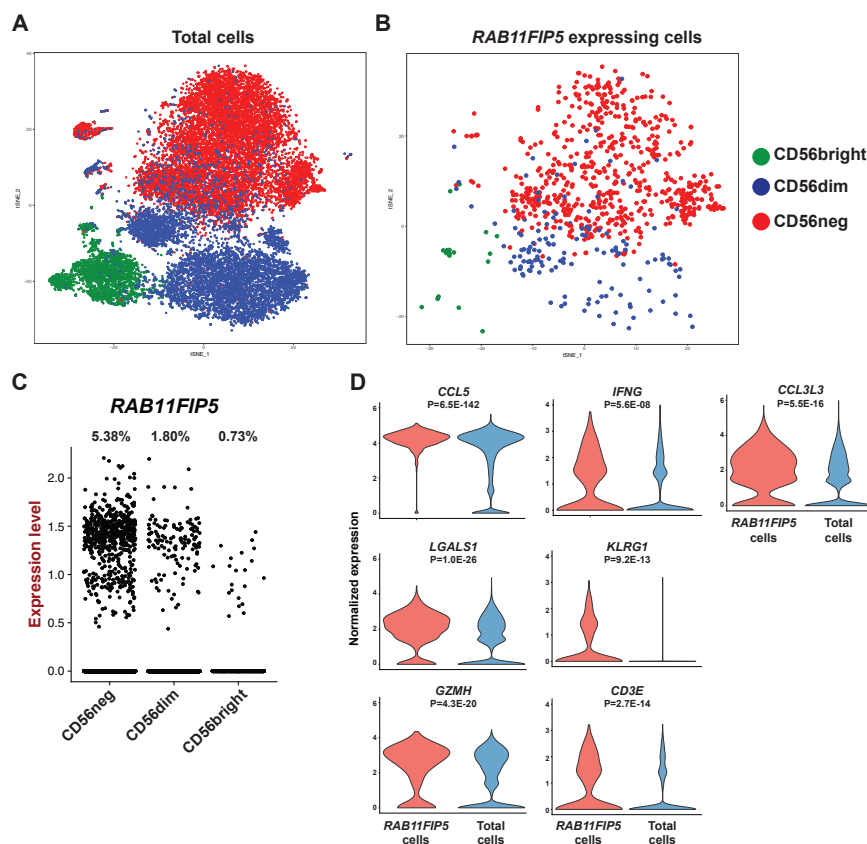
**Figure 6. High *RAB11FIP5*-Expressing Cells Are Enriched in the CD56⁻CD16⁺ NK Cell Subset**

(A and B) Non-linear dimensionality reduction by t-distributed stochastic neighbor embedding and visualization of single-cell RNA-seq of sorted NK cell subsets (CD56bright, 2,891; CD56dim, 7,674; CD56negative, 11,677) showing (A) all cells and (B) *RAB11FIP5* expressing cells. Each dot represents a single cell.

(C) Dot plot of *RAB11FIP5* expression in single cells in each NK cell subset. Normalized expression value of *RAB11FIP5* shown on y axis. Proportion of cells with detectable *RAB11FIP5* expression shown above.

(D) Violin plots of transcripts significantly (likelihood ratio test; p < 0.05) upregulated in *RAB11FIP5*-expressing cells (red) compared to cells not expressing *RAB11FIP5* (blue). Normalized transcript expression is shown on the y axis. p values for each transcript are also shown.

See also Figure S7 and Table S3.

(Sugawara et al., 2009) and in V-ATPase accumulation in duct cells in the kidney (Oehlke et al., 2011). In NK cells, Rab11 endosomes were shown to co-localize with TNF-α (Reefman et al., 2010), and Rab11 can regulate exosome formation that may play a role in killing activated CD4 T cells. (Lugini et al., 2012; Savina et al., 2002). However, the role of Rab11Fip5 in the effector function of NK cells has not previously been investigated.

In NK-92 cells, Rab11Fip5 overexpression resulted in enhanced functional responses to NK cell activation and target cell stimulation. The increased cytokine production and cytotoxic function observed in the Rab11Fip5 overexpressing cells was reproducible, but the magnitude of the change was modest and biologic relevance unclear.

We observed that the mature and CD56⁻ expanded NK cell subsets in bnAb individuals exhibited impaired functional responses to target cell stimulation despite being associated with high levels of *RAB11FIP5* expression in total PBMC. These observations suggested that Rab11Fip5 is not itself suppressive of NK function, but rather is elevated in adaptive and CD56⁻ cell subsets as a consequence of chronic stimulation. In support of this hypothesis, transcriptional profiling of canonical and adaptive subsets of NK cells in HIV-seronegative HCMV⁺ individuals identified elevation in *RAB11FIP5* in the adaptive NK subset (Lee et al., 2015). Adaptive CD56dim and CD56⁻ NK cells both have alterations in activating and inhibitory receptor expression that may diminish their activation in response to target cells (Della Chiesa et al., 2016). Moreover, lack of CD56 expression may itself contribute to NK dysfunction, as it has been suggested to have multiple roles in NK cells, including direct involvement in pathogen recognition, modulation of costimulatory signaling, and effects on NK cell maturation and migration (Mace et al., 2016; Ziegler et al., 2017). Interestingly, CD56 undergoes
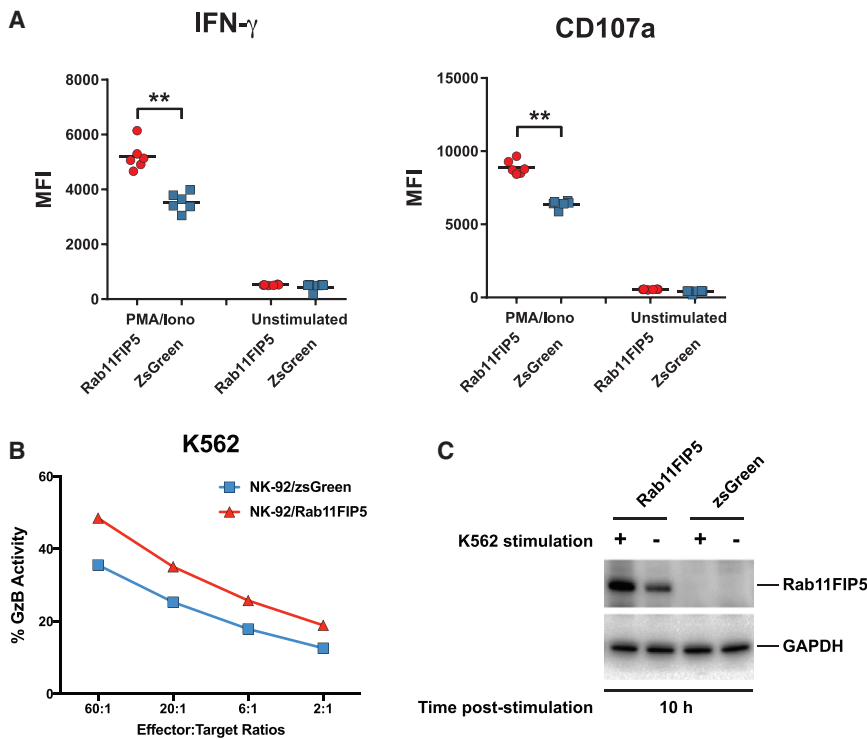
## DISCUSSION

Here, we have shown that HIV-infected individuals who developed bnAbs exhibited significantly higher transcript levels encoding the Rab11 recycling endosome targeting molecule Rab11Fip5 than those who did not. We also found increased proportions of a dysfunctional subset of NK cells in bnAb individuals that was associated with increased *RAB11FIP5* expression, and both remained significant even after correcting for the difference in viral load between the bnAb and control groups. Using *in vitro* culture systems, we found that NK cells could reduce Tfh numbers and B cell responses. Moreover, Rab11Fip5 overexpression in a NK cell line enhanced NK cell function. These observations show that NK cell dysfunction and *RAB11FIP5* expression correlate with the ability to make bnAbs in HIV-1-infected individuals and demonstrate a role for Rab11Fip5 in the regulation of NK function.

Rab11 is a GTPase associated with recycling endosomes that is involved in protein transport (Hales et al., 2001). Rab11-Fip5 is one of a family of interacting proteins (FIPs) that bind Rab11 as adaptor proteins (Hales et al., 2001; Li et al., 2014; Prekeris et al., 2000; Schonteich et al., 2008) and has been identified as a marker for poor prognosis in ovarian cancer (Willis et al., 2016) and as a candidate autism gene (Roohi et al., 2008). Rab11Fip5 is involved in transcytosis of the polymeric immunoglobulin receptor to epithelial cell surfaces (Su et al., 2010) involved in pancreatic beta cell insulin secretion

**Figure 7. Overexpression of Rab11Fip5 in NK-92 Cells Increases Cytokine and Granzyme Release**

(A) Effect of Rab11Fip5 overexpression on IFN-$\gamma$ production and degranulation (CD107a expression) of NK-92 cells in response to stimulation with PMA/ionomycin. NK-92/Rab11Fip5 (red symbols) and NK-92/ZsGreen cells (blue symbols) were stimulated with 500 ng/mL PMA and 5 $\mu$g/mL ionomycin for 2 hr in the presence of a CD107a antibody and the protein transport inhibitor monensin. Dots represent MFIs from 6 replicate wells. Significance determined by Wilcoxon-Mann-Whitney (ns, not significant; **p < 0.01).

(B) Granzyme B (GzB)-based cytotoxicity assays performed using NK-92/Rab11Fip5 (red) or NK-92/ZsGreen control (blue) cells as effectors and K562 cells as targets at different effector:target ratios. The percentage of cells positive for proteolytically active GzB is represented as % GzB activity. The average values from 3 independent experiments performed in triplicate are shown.

(C) Western blot of Rab11Fip5 expression in NK-92 cells transduced with a *RAB11FIP5* expression vector or zsGreen vector control, in the presence or absence of K562 target cell stimulation (5:1 effector:target ratio). Cells were analyzed at 10 hr post stimulation. GAPDH used as protein loading control.

See also Figure S7.

endocytosis and recycling to the plasma membrane (Diestel et al., 2007), and it has also been shown that CD56 binding to the fibroblast growth factor receptor (FGF-R) leads to Rab11-dependent endosomal recycling of FGR-R, enabling prolonged activity (Francavilla et al., 2009). If Rab11Fip5-mediated enhancement of NK cell function is mediated in part by CD56-dependent mechanisms, this may also be among the reasons that elevation of Rab11Fip5 expression in CD56$^-$ NK cells does not improve their functionality.

Adaptive-like NK expansions occur in the context of co-infection with HCMV and other viruses including HIV-1 (Brunetta et al., 2010; Gumá et al., 2006; Mela and Goodier, 2007; Peppa et al., 2018). Chronic infection with HCMV, HIV-1, and/or HCV, during which there is prolonged immune activation and exposure of NK cells to receptor-mediated activation and pro-inflammatory cytokines, is further associated with expansion of a CD56$^-$CD16$^+$ NK cell subset that has adaptive NK features but exhibits impaired degranulation and IFN$\gamma$ secretion (Alter et al., 2005; Björkström et al., 2010; Della Chiesa et al., 2012; Eller et al., 2009; Gonzalez et al., 2009; Zulu et al., 2017). Although CD56$^-$CD16$^+$ NK cells are not significantly expanded in acute HIV-1-infection (Alter et al., 2005), CD56dim NK cells start to acquire a more adaptive phenotype during HIV-1 infection, at time points preceding those when neutralizing antibody breadth typically starts to emerge (Peppa et al., 2018). Here, we have shown that dysfunction in NK cells during chronic HIV-1 infection is associated with elevation of *RAB11FIP5* expression in PBMC. Moreover, we demonstrate an association between the presence of higher proportions of CD56$^-$CD16$^+$ NK cells and bnAb generation in chronically

infected individuals with HIV-1. Although NK cell proportions and *RAB11FIP5* expression were independent of HIV-1 viral load and HCMV antibody titers, we cannot rule out that HCMV co-infection and high levels of immune activation may have played a role in the induction of NK dysfunction.

NK cells have been shown to regulate humoral responses in murine infections via reduction of CD4 Tfh availability (Cook et al., 2015; Rydyznski et al., 2015; Schuster et al., 2014), and here, we demonstrated the ability of human NK cells to reduce CD4 Tfh numbers and B cell responses in an *in vitro* NK:Tfh:B cell co-culture system. We hypothesize that NK cells reduce Tfh numbers by mediating lysis of activated CD4 Tfh, but determining the specific receptor-ligand interactions and molecular signals required for the observed NK cell inhibition of CD4 Tfh and B cell responses will require future studies. Moreover, *in vivo* studies will be required to determine how NK cells can regulate the germinal center response and whether they modulate Tfh and B cell function within germinal centers and/or act to limit CD4 Tfh numbers prior to germinal center entry. For example, NK cells were shown to migrate into follicles during SIV infection in African green monkeys to control virus replication (Huot et al., 2017). We have previously shown bnAbs frequently have long HCDR3 regions and/or polyreactivity—traits of autoantibodies (Bonsignori et al., 2014; Haynes et al., 2005; Kelsoe and Haynes, 2017). We hypothesize that the profound abnormalities in NK cell function we observed in HIV-1-infected individuals generating bnAbs may have allowed greater CD4 Tfh expansion, facilitating the development of bnAbs from tolerance-constrained B cell precursors. Interestingly, a reduction in NK cell numbers,

presence of a higher proportion of CD56$^-$ NK cells, and/or abnormalities in NK cell function have also been associated with autoantibody production in patients with autoimmune conditions including Graves' disease, Sjogren's syndrome, and rheumatoid arthritis (Akesson et al., 2010; Chalan et al., 2016; Davies et al., 2017; Witte et al., 1996; Zhang et al., 2015).

The induction of HIV-1 bnAbs in the setting of vaccination will likely require multiple strategies that include the design of Env conformations to engage rare bnAb precursor B cell receptors and sequential immunizations to select for bnAb B cell lineage maturation (Burton and Mascola, 2015; Haynes et al., 2012; Haynes and Verkoczy, 2014; Kelsoe and Haynes, 2017; Sanders and Moore, 2017). The findings in the present study suggest that bnAb induction may also be aided by down-modulation of NK activity by co-administration of inhibitors of NK cell lysis of activated CD4 T cells with HIV-1 vaccine candidates. Future work is required to identify the specific receptor-ligand interactions involved in triggering of NK cell lysis of activated Tfh cells and test whether blocking these interactions improves antibody responses during vaccination.

Thus, targeting mechanisms of recycling endosomal pathways in NK cells may not only provide insights into how to optimize HIV-1 bnAb induction but also provide strategies for harnessing control of other infectious agents and for elimination of tumor cells.

## STAR★METHODS

Detailed methods are provided in the online version of this paper and include the following:

- KEY RESOURCES TABLE
- CONTACT FOR REAGENT AND RESOURCE SHARING
- EXPERIMENTAL MODEL AND SUBJECT DETAILS
- METHOD DETAILS
  - Transcriptome sequencing of PBMCs
  - Determination of RAB11FIP5 expression in immune cell subsets
  - RNA-seq of bulk NK cells
  - Single-cell RNA sequencing of NK cell populations
  - Phenotypic and functional analysis of PBMC NK cell subsets
  - *In vitro* co-culture system to assess the ability of NK cells to reduce CD4 Tfh availability and B cell responses
  - NK-92 cell culture
  - Generation of a Rab11Fip5 stably expressing NK-92 cell line
  - Analysis of degranulation and cytokine production of RAB11FIP5-transduced NK-92 cells
  - Granzyme B-based cytotoxicity assays
- QUANTIFICATION AND STATISTICAL ANALYSIS
- DATA AND SOFTWARE AVAILABILITY

### SUPPLEMENTAL INFORMATION

Supplemental Information includes seven figures and three tables and can be found with this article online at https://doi.org/10.1016/j.cell.2018.08.064.

### REFERENCES

Akesson, C., Uvebrant, K., Oderup, C., Lynch, K., Harris, R.A., Lernmark, A., Agardh, C.D., and Cilio, C.M. (2010). Altered natural killer (NK) cell frequency and phenotype in latent autoimmune diabetes in adults (LADA) prior to insulin deficiency. Clin. Exp. Immunol. *161*, 48–56.

Alter, G., Teigen, N., Davis, B.T., Addo, M.M., Suscovich, T.J., Waring, M.T., Streeck, H., Johnston, M.N., Staller, K.D., Zaman, M.T., et al. (2005). Sequential deregulation of NK cell subset distribution and function starting in acute HIV-1 infection. Blood *106*, 3366–3369.

Anders, S., Pyl, P.T., and Huber, W. (2015). HTSeq–a Python framework to work with high-throughput sequencing data. Bioinformatics *31*, 166–169.

Béziat, V., Descours, B., Parizot, C., Debré, P., and Vieillard, V. (2010). NK cell terminal differentiation: correlated stepwise decrease of NKG2A and acquisition of KIRs. PLoS ONE *5*, e11966.

Björkström, N.K., Ljunggren, H.G., and Sandberg, J.K. (2010). CD56 negative NK cells: origin, function, and role in chronic viral disease. Trends Immunol. *31*, 401–406.

Bolger, A.M., Lohse, M., and Usadel, B. (2014). Trimmomatic: a flexible trimmer for Illumina sequence data. Bioinformatics *30*, 2114–2120.

Bonsignori, M., Wiehe, K., Grimm, S.K., Lynch, R., Yang, G., Kozink, D.M., Perrin, F., Cooper, A.J., Hwang, K.K., Chen, X., et al. (2014). An autoreactive antibody from an SLE/HIV-1 individual broadly neutralizes HIV-1. J. Clin. Invest. *124*, 1835–1843.

Borrow, P., and Moody, M.A. (2017). Immunologic characteristics of HIV-infected individuals who make broadly neutralizing antibodies. Immunol. Rev. *275*, 62–78.

Bradley, T., Fera, D., Bhiman, J., Eslamizar, L., Lu, X., Anasti, K., Zhang, R., Sutherland, L.L., Scearce, R.M., Bowman, C.M., et al. (2016). Structural

constraints of vaccine-induced tier-2 autologous HIV neutralizing antibodies targeting the receptor-binding site. Cell Rep. *14*, 43–54.

Brunetta, E., Fogli, M., Varchetta, S., Bozzo, L., Hudspeth, K.L., Marcenaro, E., Moretta, A., and Mavilio, D. (2010). Chronic HIV-1 viremia reverses NKG2A/NKG2C ratio on natural killer cells in patients with human cytomegalovirus co-infection. AIDS *24*, 27–34.

Burton, D.R., and Mascola, J.R. (2015). Antibody responses to envelope glycoproteins in HIV-1 infection. Nat. Immunol. *16*, 571–576.

Chalan, P., Bijzet, J., Kroesen, B.J., Boots, A.M., and Brouwer, E. (2016). Altered natural killer cell subsets in seropositive arthralgia and early rheumatoid arthritis are associated with autoantibody status. J. Rheumatol. *43*, 1008–1016.

Cook, K.D., Kline, H.C., and Whitmire, J.K. (2015). NK cells inhibit humoral immunity by reducing the abundance of CD4+ T follicular helper cells during a chronic virus infection. J. Leukoc. Biol. *98*, 153–162.

Davies, R., Hammenfors, D., Bergum, B., Jakobsen, K., Solheim, M., Vogelsang, P., Brun, J.G., Bryceson, Y., Jonsson, R., and Appel, S. (2017). Patients with primary Sjögren's syndrome have alterations in absolute quantities of specific peripheral leucocyte populations. Scand. J. Immunol. *86*, 491–502.

Della Chiesa, M., Falco, M., Podestà, M., Locatelli, F., Moretta, L., Frassoni, F., and Moretta, A. (2012). Phenotypic and functional heterogeneity of human NK cells developing after umbilical cord blood transplantation: a role for human cytomegalovirus? Blood *119*, 399–410.

Della Chiesa, M., Pesce, S., Muccio, L., Carlomagno, S., Sivori, S., Moretta, A., and Marcenaro, E. (2016). Features of memory-like and PD-1(+) human NK cell subsets. Front. Immunol. *7*, 351.

Diestel, S., Schaefer, D., Cremer, H., and Schmitz, B. (2007). NCAM is ubiquitylated, endocytosed and recycled in neurons. J. Cell Sci. *120*, 4035–4049.

Dobin, A., Davis, C.A., Schlesinger, F., Drenkow, J., Zaleski, C., Jha, S., Batut, P., Chaisson, M., and Gingeras, T.R. (2013). STAR: ultrafast universal RNA-seq aligner. Bioinformatics *29*, 15–21.

Doria-Rose, N.A., Klein, R.M., Daniels, M.G., O'Dell, S., Nason, M., Lapedes, A., Bhattacharya, T., Migueles, S.A., Wyatt, R.T., Korber, B.T., et al. (2010). Breadth of human immunodeficiency virus-specific neutralizing activity in sera: clustering analysis and association with clinical variables. J. Virol. *84*, 1631–1636.

Eller, M.A., Eller, L.A., Ouma, B.J., Thelian, D., Gonzalez, V.D., Guwatudde, D., McCutchan, F.E., Marovich, M.A., Michael, N.L., de Souza, M.S., et al. (2009). Elevated natural killer cell activity despite altered functional and phenotypic profile in Ugandans with HIV-1 clade A or clade D infection. J. Acquir. Immune Defic. Syndr. *51*, 380–389.

Fauci, A.S., Mavilio, D., and Kottilil, S. (2005). NK cells in HIV infection: paradigm for protection or targets for ambush. Nat. Rev. Immunol. *5*, 835–843.

Foley, B., Cooley, S., Verneris, M.R., Pitt, M., Curtsinger, J., Luo, X., Lopez-Vergès, S., Lanier, L.L., Weisdorf, D., and Miller, J.S. (2012). Cytomegalovirus reactivation after allogeneic transplantation promotes a lasting increase in educated NKG2C+ natural killer cells with potent function. Blood *119*, 2665–2674.

Francavilla, C., Cattaneo, P., Berezin, V., Bock, E., Ami, D., de Marco, A., Christofori, G., and Cavallaro, U. (2009). The binding of NCAM to FGFR1 induces a specific cellular response mediated by receptor trafficking. J. Cell Biol. *187*, 1101–1116.

Gianchecchi, E., Delfino, D.V., and Fierabracci, A. (2018). NK cells in autoimmune diseases: Linking innate and adaptive immune responses. Autoimmun. Rev. *17*, 142–154.

Gonzalez, V.D., Falconer, K., Björkström, N.K., Blom, K.G., Weiland, O., Ljunggren, H.G., Alaeus, A., and Sandberg, J.K. (2009). Expansion of functionally skewed CD56-negative NK cells in chronic hepatitis C virus infection: correlation with outcome of pegylated IFN-alpha and ribavirin treatment. J. Immunol. *183*, 6612–6618.

Gumá, M., Cabrera, C., Erkizia, I., Bofill, M., Clotet, B., Ruiz, L., and López-Botet, M. (2006). Human cytomegalovirus infection is associated with increased proportions of NK cells that express the CD94/NKG2C receptor in aviremic HIV-1-positive patients. J. Infect. Dis. *194*, 38–41.

Hales, C.M., Griner, R., Hobdy-Henderson, K.C., Dorn, M.C., Hardy, D., Kumar, R., Navarre, J., Chan, E.K., Lapierre, L.A., and Goldenring, J.R. (2001). Identification and characterization of a family of Rab11-interacting proteins. J. Biol. Chem. *276*, 39067–39075.

Hayakawa, Y., and Smyth, M.J. (2006). CD27 dissects mature NK cells into two subsets with distinct responsiveness and migratory capacity. J. Immunol. *176*, 1517–1524.

Haynes, B.F., and Burton, D.R. (2017). Developing an HIV vaccine. Science *355*, 1129–1130.

Haynes, B.F., and Mascola, J.R. (2017). The quest for an antibody-based HIV vaccine. Immunol. Rev. *275*, 5–10.

Haynes, B.F., and Verkoczy, L. (2014). AIDS/HIV. Host controls of HIV neutralizing antibodies. Science *344*, 588–589.

Haynes, B.F., Fleming, J., St Clair, E.W., Katinger, H., Stiegler, G., Kunert, R., Robinson, J., Scearce, R.M., Plonk, K., Staats, H.F., et al. (2005). Cardiolipin polyspecific autoreactivity in two broadly neutralizing HIV-1 antibodies. Science *308*, 1906–1908.

Haynes, B.F., Kelsoe, G., Harrison, S.C., and Kepler, T.B. (2012). B-cell-lineage immunogen design in vaccine development with HIV-1 as a case study. Nat. Biotechnol. *30*, 423–433.

Huot, N., Jacquelin, B., Garcia-Tellez, T., Rascle, P., Ploquin, M.J., Madec, Y., Reeves, R.K., Derreudre-Bosquet, N., and Müller-Trutwin, M. (2017). Natural killer cells migrate into and control simian immunodeficiency virus replication in lymph node follicles in African green monkeys. Nat. Med. *23*, 1277–1286.

Kelsoe, G., and Haynes, B.F. (2017). Host controls of HIV broadly neutralizing antibody development. Immunol. Rev. *275*, 79–88.

Klasse, P.J., LaBranche, C.C., Ketas, T.J., Ozorowski, G., Cupo, A., Pugach, P., Ringe, R.P., Golabek, M., van Gils, M.J., Guttman, M., et al. (2016). Sequential and simultaneous immunization of rabbits with HIV-1 envelope glycoprotein SOSIP.664 trimers from clades A, B and C. PLoS Pathog. *12*, e1005864.

Langmead, B., and Salzberg, S.L. (2012). Fast gapped-read alignment with Bowtie 2. Nat. Methods *9*, 357–359.

Lee, J., Zhang, T., Hwang, I., Kim, A., Nitschke, L., Kim, M., Scott, J.M., Kamimura, Y., Lanier, L.L., and Kim, S. (2015). Epigenetic modification and antibody-dependent expansion of memory-like NK cells in human cytomegalovirus-infected individuals. Immunity *42*, 431–442.

Li, D., Mangan, A., Cicchini, L., Margolis, B., and Prekeris, R. (2014). FIP5 phosphorylation during mitosis regulates apical trafficking and lumenogenesis. EMBO Rep. *15*, 428–437.

Liao, H.X., Tsao, C.Y., Alam, S.M., Muldoon, M., Vandergrift, N., Ma, B.J., Lu, X., Sutherland, L.L., Scearce, R.M., Bowman, C., et al. (2013). Antigenicity and immunogenicity of transmitted/founder, consensus, and chronic envelope glycoproteins of human immunodeficiency virus type 1. J. Virol. *87*, 4185–4201.

Locci, M., Havenar-Daughton, C., Landais, E., Wu, J., Kroenke, M.A., Arlehamn, C.L., Su, L.F., Cubas, R., Davis, M.M., Sette, A., et al.; International AIDS Vaccine Initiative Protocol C Principal Investigators (2013). Human circulating PD-1+CXCR3-CXCR5+ memory Tfh cells are highly functional and correlate with broadly neutralizing HIV antibody responses. Immunity *39*, 758–769.

Lopez-Vergès, S., Milush, J.M., Schwartz, B.S., Pando, M.J., Jarjoura, J., York, V.A., Houchins, J.P., Miller, S., Kang, S.M., Norris, P.J., et al. (2011). Expansion of a unique CD57+NKG2Chi natural killer cell subset during acute human cytomegalovirus infection. Proc. Natl. Acad. Sci. USA *108*, 14725–14732.

Love, M.I., Huber, W., and Anders, S. (2014). Moderated estimation of fold change and dispersion for RNA-seq data with DESeq2. Genome Biol. *15*, 550.

Lugini, L., Cecchetti, S., Huber, V., Luciani, F., Macchia, G., Spadaro, F., Paris, L., Abalsamo, L., Colone, M., Molinari, A., et al. (2012). Immune surveillance properties of human NK cell-derived exosomes. J. Immunol. *189*, 2833–2842.

Mace, E.M., Gunesch, J.T., Dixon, A., and Orange, J.S. (2016). Human NK cell development requires CD56-mediated motility and formation of the developmental synapse. Nat. Commun. 7, 12171.

Mah, A.Y., and Cooper, M.A. (2016). Metabolic regulation of natural killer cell IFN-γ production. Crit. Rev. Immunol. 36, 131–147.

Mavilio, D., Benjamin, J., Daucher, M., Lombardo, G., Kottilil, S., Planta, M.A., Marcenaro, E., Bottino, C., Moretta, L., Moretta, A., and Fauci, A.S. (2003). Natural killer cells in HIV-1 infection: dichotomous effects of viremia on inhibitory and activating receptors and their functional correlates. Proc. Natl. Acad. Sci. USA 100, 15011–15016.

McCoy, L.E., and Burton, D.R. (2017). Identification and specificity of broadly neutralizing antibodies against HIV. Immunol. Rev. 275, 11–20.

McDavid, A., Finak, G., Chattopadyay, P.K., Dominguez, M., Lamoreaux, L., Ma, S.S., Roederer, M., and Gottardo, R. (2013). Data exploration, quality control and testing in single-cell qPCR-based gene expression experiments. Bioinformatics 29, 461–467.

Mela, C.M., and Goodier, M.R. (2007). The contribution of cytomegalovirus to changes in NK cell receptor expression in HIV-1-infected individuals. J. Infect. Dis. 195, 158–160.

Moody, M.A., Pedroza-Pacheco, I., Vandergrift, N.A., Chui, C., Lloyd, K.E., Parks, R., Soderberg, K.A., Ogbe, A.T., Cohen, M.S., Liao, H.X., et al. (2016). Immune perturbations in HIV-1-infected individuals who make broadly neutralizing antibodies. Sci. Immunol. 1, aag0851.

Oehlke, O., Martin, H.W., Osterberg, N., and Roussa, E. (2011). Rab11b and its effector Rip11 regulate the acidosis-induced traffic of V-ATPase in salivary ducts. J. Cell. Physiol. 226, 638–651.

Pauthner, M., Havenar-Daughton, C., Sok, D., Nkolola, J.P., Bastidas, R., Boopathy, A.V., Carnathan, D.G., Chandrashekar, A., Cirelli, K.M., Cottrell, C.A., et al. (2017). Elicitation of robust tier 2 neutralizing antibody responses in nonhuman primates by HIV envelope trimer immunization using optimized approaches. Immunity 46, 1073–1088.

Peppa, D., Pedroza-Pacheco, I., Pellegrino, P., Williams, I., Maini, M.K., and Borrow, P. (2018). Adaptive reconfiguration of natural killer cells in HIV-1 infection. Front. Immunol. 9, 474.

Pollara, J., Hart, L., Brewer, F., Pickeral, J., Packard, B.Z., Hoxie, J.A., Komoriya, A., Ochsenbauer, C., Kappes, J.C., Roederer, M., et al. (2011). High-throughput quantitative analysis of HIV-1 and SIV-specific ADCC-mediating antibody responses. Cytometry A 79, 603–612.

Prekeris, R., Klumperman, J., and Scheller, R.H. (2000). A Rab11/Rip11 protein complex regulates apical membrane trafficking via recycling endosomes. Mol. Cell 6, 1437–1448.

Reefman, E., Kay, J.G., Wood, S.M., Offenhäuser, C., Brown, D.L., Roy, S., Stanley, A.C., Low, P.C., Manderson, A.P., and Stow, J.L. (2010). Cytokine secretion is distinct from secretion of cytotoxic granules in NK cells. J. Immunol. 184, 4852–4862.

Roberts, A., Trapnell, C., Donaghey, J., Rinn, J.L., and Pachter, L. (2011). Improving RNA-seq expression estimates by correcting for fragment bias. Genome Biol. 12, R22.

Roohi, J., Tegay, D.H., Pomeroy, J.C., Burkett, S., Stone, G., Stanyon, R., and Hatchwell, E. (2008). A de novo apparently balanced translocation [46,XY,t(2;9)(p13;p24)] interrupting RAB11FIP5 identifies a potential candidate gene for autism spectrum disorder. Am. J. Med. Genet. B. Neuropsychiatr. Genet. 147B, 411–417.

Rydyznski, C.E., and Waggoner, S.N. (2015). Boosting vaccine efficacy the natural (killer) way. Trends Immunol. 36, 536–546.

Rydyznski, C., Daniels, K.A., Karmele, E.P., Brooks, T.R., Mahl, S.E., Moran, M.T., Li, C., Sutiwisesak, R., Welsh, R.M., and Waggoner, S.N. (2015). Generation of cellular immune memory and B-cell immunity is impaired by natural killer cells. Nat. Commun. 6, 6375.

Sanders, R.W., and Moore, J.P. (2017). Native-like Env trimers as a platform for HIV-1 vaccine design. Immunol. Rev. 275, 161–182.

Satija, R., Farrell, J.A., Gennert, D., Schier, A.F., and Regev, A. (2015). Spatial reconstruction of single-cell gene expression data. Nat. Biotechnol. 33, 495–502.

Saunders, K.O., Verkoczy, L.K., Jiang, C., Zhang, J., Parks, R., Chen, H., Housman, M., Bouton-Verville, H., Shen, X., Trama, A.M., et al. (2017). Vaccine induction of heterologous tier 2 HIV-1 neutralizing antibodies in animal models. Cell Rep. 21, 3681–3690.

Savina, A., Vidal, M., and Colombo, M.I. (2002). The exosome pathway in K562 cells is regulated by Rab11. J. Cell Sci. 115, 2505–2515.

Schlums, H., Cichocki, F., Tesi, B., Theorell, J., Beziat, V., Holmes, T.D., Han, H., Chiang, S.C., Foley, B., Mattsson, K., et al. (2015). Cytomegalovirus infection drives adaptive epigenetic diversification of NK cells with altered signaling and effector function. Immunity 42, 443–456.

Schonteich, E., Wilson, G.M., Burden, J., Hopkins, C.R., Anderson, K., Goldenring, J.R., and Prekeris, R. (2008). The Rip11/Rab11-FIP5 and kinesin II complex regulates endocytic protein recycling. J. Cell Sci. 121, 3824–3833.

Schuster, I.S., Wikstrom, M.E., Brizard, G., Coudert, J.D., Estcourt, M.J., Manzur, M., O'Reilly, L.A., Smyth, M.J., Trapani, J.A., Hill, G.R., et al. (2014). TRAIL+ NK cells control CD4+ T cell responses during chronic viral infection to limit autoimmunity. Immunity 41, 646–656.

Su, T., Bryant, D.M., Luton, F., Vergés, M., Ulrich, S.M., Hansen, K.C., Datta, A., Eastburn, D.J., Burlingame, A.L., Shokat, K.M., and Mostov, K.E. (2010). A kinase cascade leading to Rab11-FIP5 controls transcytosis of the polymeric immunoglobulin receptor. Nat. Cell Biol. 12, 1143–1153.

Sugawara, K., Shibasaki, T., Mizoguchi, A., Saito, T., and Seino, S. (2009). Rab11 and its effector Rip11 participate in regulation of insulin granule exocytosis. Genes Cells 14, 445–456.

Takeda, K., Cretney, E., Hayakawa, Y., Ota, T., Akiba, H., Ogasawara, K., Yagita, H., Kinoshita, K., Okumura, K., and Smyth, M.J. (2005). TRAIL identifies immature natural killer cells in newborn mice and adult mouse liver. Blood 105, 2082–2089.

Waggoner, S.N., Reighard, S.D., Gyurova, I.E., Cranert, S.A., Mahl, S.E., Karmele, E.P., McNally, J.P., Moran, M.T., Brooks, T.R., Yaqoob, F., and Rydyznski, C.E. (2016). Roles of natural killer cells in antiviral immunity. Curr. Opin. Virol. 16, 15–23.

Willis, S., Villalobos, V.M., Gevaert, O., Abramovitz, M., Williams, C., Sikic, B.I., and Leyland-Jones, B. (2016). Single gene prognostic biomarkers in ovarian cancer: a meta-analysis. PLoS ONE 11, e0149183.

Witte, T., Bode, F.M., Hammer, M., Deicher, H., and Schmidt, R.E. (1996). Autoantibody against a 58 kD molecule in a patient with neutropenia and NK cell deficiency. Br. J. Haematol. 92, 565–570.

Zhang, Y., Lv, G., Lou, X., Peng, D., Qu, X., Yang, X., Ayana, D.A., Guo, H., and Jiang, Y. (2015). NKG2A expression and impaired function of NK cells in patients with new onset of Graves' disease. Int. Immunopharmacol. 24, 133–139.

Zheng, G.X., Terry, J.M., Belgrader, P., Ryvkin, P., Bent, Z.W., Wilson, R., Ziraldo, S.B., Wheeler, T.D., McDermott, G.P., Zhu, J., et al. (2017). Massively parallel digital transcriptional profiling of single cells. Nat. Commun. 8, 14049.

Ziegler, S., Weiss, E., Schmitt, A.L., Schlegel, J., Burgert, A., Terpitz, U., Sauer, M., Moretta, L., Sivori, S., Leonhardt, I., et al. (2017). CD56 is a pathogen recognition receptor on human natural killer cells. Sci. Rep. 7, 6138.

Zulu, M.Z., Naidoo, K.K., Mncube, Z., Jaggernath, M., Goulder, P.J.R., Ndung'u, T., Altfeld, M., and Thobakgale, C.F. (2017). Reduced expression of Siglec-7, NKG2A, and CD57 on terminally differentiated CD56⁻CD16⁺ natural killer cell subset is associated with natural killer cell dysfunction in chronic HIV-1 clade C infection. AIDS Res. Hum. Retroviruses 33, 1205–1213.

# STAR★METHODS

## KEY RESOURCES TABLE

| REAGENT or RESOURCE | SOURCE | IDENTIFIER |
|---|---|---|
| Antibodies | | |
| PE-Texas Red Mouse Anti-Human CD3, Clone 7D6 | Thermo Fisher | Cat#MHCD0317; RRID: AB_10376002 |
| PE Mouse Anti-Human CD4, Clone SK3 | BD Biosciences | Cat#345769; RRID: AB_2728699 |
| BV650 Mouse Anti-Human CD19, Clone HIB19 | Biolegend | Cat# 302238; RRID: AB_2562097 |
| PE/Cy5 Mouse Anti-Human CD20, Clone 2H7 | Biolegend | Cat# 302308; RRID: AB_314256 |
| BV711 Mouse Anti-Human CD27, Clone O323 | Biolegend | Cat# 302834; RRID: AB_2563809 |
| BV785 Mouse Anti-Human CD38, Clone HIT2 | Biolegend | Cat# 303530; RRID: AB_2565893 |
| BV605 Mouse Anti-Human CD56, Clone NCAM16.2 | BD Biosciences | Cat# 562780; RRID: AB_2728700 |
| PE/Cy7 Mouse Anti-Human IgD, Clone IA6-2 | Biolegend | Cat# 348210; RRID: AB_10680462 |
| Alexa Fluor 647 Mouse Anti-Human IgM, Clone MHM-88 | Biolegend | Cat# 314535; RRID: AB_2566612 |
| PerCP anti-human CD16 antibody, Clone 3G8 | Biolegend | Cat# 302030; RRID: AB_940380 |
| Brilliant Violet 711 anti-human CD16 antibody, Clone 3G8 | Biolegend | Cat# 302044; RRID: AB_2563802 |
| CD159a (NKG2a) Antibody, Clone Z199 | Beckman Coulter | Cat# B10246; RRID: AB_2687887 |
| Mouse Anti-Human Nkg2c Monoclonal antibody, Phycoerythrin Conjugated, Clone 134591 | R and D Systems | Cat# FAB138P; RRID: AB_2132983 |
| CD4 Monoclonal Antibody, APC-eFluor 780, Clone RPA-T4 | eBioscience, Thermo Fisher Scientific | Cat# 47-0049-42; RRID: AB_1272044 |
| CD8a Monoclonal Antibody, Alexa Fluor 700, Clone OKT8 | eBioscience, Thermo Fisher Scientific | Cat# 56-0086-42; RRID: AB_10670753 |
| Brilliant Violet 650 anti-human CD3 antibody, Clone OKT3 | Biolegend | Cat# 317324; RRID: AB_2563352 |
| Brilliant Violet 711 anti-human CD279 (PD-1) antibody, Clone EH12.2H7 | Biolegend | Cat# 329928; RRID: AB_2562911 |
| BV605 Mouse Anti-Human CD57 antibody, Clone NK-1 | BD Biosciences | Cat# 563895; RRID: AB_2632390 |
| PE/Dazzle 594 anti-human CD56 (NCAM) antibody, Clone HCD56 | Biolegend | Cat# 318348; RRID: AB_2563564 |
| Human PLZF Allophycocyanin mAb (Clone 6318100) antibody | R and D Systems | Cat# IC2944A; RRID: AB_10730709 |
| Milli-Mark Anti-Fc RI, subunit-FITC antibody, Polyclonal Antibody | Millipore | Cat# FCABS400F; RRID: AB_11203492 |
| PE anti-human CD328 (Siglec-7) antibody, Clone 6-434 | Biolegend | Cat# 339204; RRID: AB_1501160 |
| Mouse Anti-Human CD158e (KIR3DL1) Monoclonal Antibody, APC Conjugated Clone DX9 | Miltenyi Biotec | Cat# 130-092-474; RRID: AB_871612 |
| Human KIR2DL1/CD158a Allophycocyanin mAb (Clone 143211) antibody | R and D Systems | Cat# FAB1844A; RRID: AB_416855 |
| APC CD158b1/b2,j Clone GL18 | Beckman Coulter | Cat#A22333 |
| Human KIR3DL2/CD158k APC-conjugated Antibody, Clone # 539304 | R and D Systems | Cat# FAB2878A |
| Biotin anti-human CD85j (ILT2) antibody, Clone GHI/75 | Biolegend | Cat# 333706; RRID: AB_1089083 |
| Brilliant Violet 510 anti-human CD14 antibody, Clone M5E2 | Biolegend | Cat# 301842; RRID: AB_2561946 |

(*Continued on next page*)

*Continued*

| REAGENT or RESOURCE | SOURCE | IDENTIFIER |
|---|---|---|
| Brilliant Violet 510 anti-human CD19 antibody, Clone HIB19 | Biolegend | Cat# 302242; RRID: AB_2561668 |
| Brilliant Violet 421 Mouse Anti-Human IFN-$\gamma$ antibody, Clone B27 | BD Biosciences | Cat#562988; RRID: AB_2737934 |
| Alexa Fluor 647 Mouse Anti-Human IFN-$\gamma$ antibody, Clone 4S.B3 | BD Biosciences | Cat# 502516; RRID: AB_493031 |
| Brilliant Violet 711 anti-human TNF-a antibody, Clone MAb11 | Biolegend | Cat# 502940; RRID: AB_2563885 |
| PE/Cy7 anti-human TNF-a antibody, Clone MAb11 | Biolegend | Cat# 502930; RRID: AB_2204079 |
| APC-H7 Mouse Anti-human CD107a antibody, Clone H4A3 | BD Biosciences | Cat# 561343; RRID: AB_10644020 |
| Brilliant Violet 711 Mouse Anti-human CD107a antibody, Clone H4A3 | Biolegend | Cat# 328640; RRID: AB_2565840 |
| FITC anti-human/mouse Granzyme B antibody, Clone GB11 | Biolegend | Cat# 515403; RRID: AB_2114575 |
| PE anti-human Perforin antibody, Clone B-D48 | Biolegend | Cat# 353304; RRID: AB_2616860 |
| Rabbit anti-human Rab11FIP5 polyclonal antibody | Sigma | Cat# HPA036407; RRID: AB_10669778 |
| HRP conjugated anti-GAPDH Monoclonal Antibody, Clone GA1R | Thermo Fisher Scientific | Cat# MA5-15738-HRP; RRID: AB_2537659 |
| PerCP-Cy5.5 anti-human CD19, clone SJ25C1 | Biolegend | Cat# 363016; RRID: AB_2564204 |
| PE-Texas RED anti-human CD3d, clone 7D6 | Thermo Fisher | Cat# MHCD0317; RRID: AB_10376002 |
| APC-H7 anti-human CD4, clone SK3 | BD Biosciences | Cat# 641407; RRID: AB_1645733 |
| Brilliant Violet 570 anti-human CD8a, clone RPA-T8 | Biolegend | Cat#301038; RRID: AB_2563213 |
| Brilliant Violet 650 anti-human CD56, clone HCD56 | Biolegend | Cat# 318344; RRID: AB_2563838 |
| Pacific Blue anti-human CD14, clone M5E2 | Biolegend | Cat# 301815; RRID: AB_493163 |
| Brilliant Violet 570 anti-human CD16, clone 3G8 | Biolegend | Cat# 302036; RRID: AB_2632790 |
| Alexa Fluor 488 anti-human CD11c, clone 3.9 | Biolegend | Cat# 301618; RRID: AB_439791 |
| PE-Cy7 anti-human CD123, clone 6H6 | Biolegend | Cat# 306010; RRID: AB_493576 |
| APC anti-human CD8, clone RPA-T8 | BD Biosciences | Cat# 555369; RRID: AB_398595 |
| Alexa Fluor 700 anti-human HLA-DR, clone L243 | Biolegend | Cat# 307626; RRID: AB_493771 |
| Biological Samples | | |
| Cohort A human samples (deidentified) | Moody et al., 2016 | N/A |
| Cohort B human samples (deidentified) | Doria-Rose et al., 2010 | N/A |
| Chemicals, Peptides, and Recombinant Proteins | | |
| *Brilliant Violet 711 Streptavidin* | Biolegend | Cat#405241 |
| Staphylococcal enterotoxin B from Staphylococcus aureus | Sigma | Cat# S4881 |
| PMA | Sigma | Cat# P1585 |
| Ionomycin | Sigma | Cat# I9657 |
| LIVE/DEAD Fixable Red Dead Cell Stain Kit | Thermo Fisher Scientific | Cat#L34972 |
| LIVE/DEAD Fixable Aqua Dead Cell Stain Kit | Thermo Fisher Scientific | Cat#L34957 |
| Recombinant Human IL-2 Aldesleukin Proleukin | Novartis | N/A |
| Recombinant IL-2 | PeproTech | Cat# 200-02 |
| Recombinant Human IL-12 p70 | PeproTech | Cat#200-12 |
| Recombinant Human IL-15 | Miltenyi | Cat#130-093-955 |
| Recombinant Human IL-18 | MBL | Cat#B001-5 |
| Human TruStain FcX | Biolegend | Cat#422302 |

*(Continued on next page)*

**Continued**

| REAGENT or RESOURCE | SOURCE | IDENTIFIER |
|---|---|---|
| Parafolmadehyde solution 4% PBS | Santa Cruz | Cat#SC-281692 |
| BD GolgiStop Protein Transport Inhibitor (Containing Monensin) | BD Biosciences | Cat#554724 |
| BD GolgiPlug Protein Transport Inhibitor (Containing Brefeldin A) | BD Biosciences | Cat#555029 |
| Critical Commercial Assays | | |
| Foxp3 Transcription Factor Staining Buffer Set | ThermoFisher Scientific | Cat# 00-5523-00 |
| CellTrace Violet Cell Proliferation kit | ThermoFisher Scientific | Cat#C34571 |
| Naive B cell isolation kit II | Miltenyi | Cat#130-091-150 |
| NK cell isolation kit | Miltenyi | Cat# 130-092-657 |
| CD4 T cell isolation kit | Miltenyi | Cat#130-096-533 |
| CountBright absolute counting beads | ThermoFisher Scientific | Cat#C36950 |
| Human IgM ELISA development kit (ALP) | MabTech | Cat#3880-1AD-6 |
| Human IgG ELISA development kit (ALP) | MabTech | Cat#3850-1AD-6 |
| MILLIPLEX MAP Human CD8+ T Cell PREMIXED Magnetic Bead Panel | Millipore | Cat# HCD8MAG15K17PMX |
| Target Cell marker TFL4 | OncoImmunin | Cat# TFL4 |
| Viability marker NFL1 | OncoImmunin | Cat# NFL1 |
| Granzyme B substrate | OncoImmunin | Cat# GranToxiLux |
| Alpha Minimum Essential medium | GIBCO | Cat# 12561072 |
| L-glutamine | GIBCO | Cat# 25030081 |
| Inositol | Sigma | Cat# I5125 |
| 2-Mercaptoethanol | GIBCO | Cat# 31350010 |
| Folic acid | Sigma | Cat# F7876 |
| Horse serum (GIBCO, Catlog#16050122) | GIBCO | Cat# 16050122 |
| Fetal bovine serum (GIBCO, Catlog#10099141). | GIBCO | Cat# 10099141 |
| CMV IgG EIA | Biorad | 25177 |
| CMV IgM EIA | Biorad | 25178 |
| RNeasy mini kit | QIAGEN | 79656 |
| TruSeq stranded mRNA kit | Illumina | 20020595 |
| RNeasy micro kit | QIAGEN | 74034 |
| High-Capacity RNA-To-cDNA Kit | ThermoFisher | 4387406 |
| *RAB11FIP5* Taqman probe | ThermoFisher | Hs00392033_ml |
| *GAPDH* Taqman probe | ThermoFisher | Hs03929097_gl |
| SmartSeq Ultra-low v4 kit | Takara Bio USA | 634891 |
| Nextera XT library kit | Illumina | FC-131-1096 |
| Universal library quantification kit | Kapa Biosystems | KK4828 |
| NextSeq500 Hi-Output kit v2 | Illumina | FC-404-2002 |
| Chromium SingleCell 3′ library and gel bead kit | 10X Genomics | 120237 |
| Deposited Data | | |
| Bulk RNA-seq data | NCBI Gene Expression Omnibus | GEO: GSE115449 |
| Single-cell RNA-seq data | NCBI Sequence Read Archive | SRA: SRP150325 |
| Experimental Models: Cell Lines | | |
| NK-92 human NK cell line | ATCC | CRL-2407 |
| Lenti-X 293T Cell Line | Clontech | Cat# 632180 |

**Continued**

| REAGENT or RESOURCE | SOURCE | IDENTIFIER |
|---|---|---|
| K562 | ATCC | CCL-243 |
| 721.221 | ATCC | CRL-1855 |
| Recombinant DNA | | |
| Human Rab11FIP5 gene | Genscript | NCBI ACCESSION# NM_015470.2 |
| pLVX-IRES-ZsGreen1 | Clontech | Cat# 632187 |
| pMD2.G | Addgene | Cat#12259 |
| psPAX2 | Addgene | Cat# 12260 |
| Software and Algorithms | | |
| Diva | BD Biosciences | http://www.bdbiosciences.com/us/instruments/clinical/software/flow-cytometry-acquisition/bd-facsdiva-software/m/333333/overview |
| FlowJo (version 9.9.4) | FlowJo, LLC | https://www.flowjo.com |
| GraphPad Prism (version 7.0) | GraphPad Software | https://www.graphpad.com/scientific-software/prism/ |
| Cytobank MRC | Cytobank Inc | http://Mrc.cytobank.org |
| SPICE Version 5.35 (5.35001) | National Institute of Allergy and Infectious Diseases | https://exon.niaid.nih.gov/spice/ |
| Trimmomatic | Bolger et al., 2014 | N/A |
| Bowtie2 | Langmead and Salzberg, 2012 | N/A |
| Express | Roberts et al., 2011 | N/A |
| Trim Galore | N/A | http://www.bioinformatics.babraham.ac.uk/projects/trim_galore/ |
| STAR | Dobin et al., 2013 | N/A |
| HTseq | Anders et al., 2015 | N/A |
| DeSeq2 | Love et al., 2014 | N/A |
| Ingenuity Pathway Analysis | QIAGEN | N/A |
| CellRanger | Zheng et al., 2017 | N/A |
| Seurat | Satija et al., 2015 | N/A |
| SAS v9.4 | SAS Institute | N/A |

## CONTACT FOR REAGENT AND RESOURCE SHARING

Further information and requests for resources and reagents should be directed to and will be fulfilled by the lead contact, Todd Bradley (todd.bradley@duke.edu).

## EXPERIMENTAL MODEL AND SUBJECT DETAILS

Deidentified samples were utilized from two existing cohorts that were previously described (Doria-Rose et al., 2010; Moody et al., 2016). Other details and exact number of subjects utilized are indicated in the Results section and Figure S1A. Both studies were approved by the Duke Medicine and National Institutes of Health Institution Review Boards as well as the ethics boards of the local sites.

## METHOD DETAILS

### Transcriptome sequencing of PBMCs

Cryopreserved PBMCs from 95 subjects were thawed and total RNA was isolated using RNeasy mini kit according the manufacturer's protocol (QIAGEN). Library preparation for Illumina sequencing was performed using the TruSeq stranded mRNA kit (Illumina) and sequenced to a depth of at least 50 million reads per sample with 2x50bp read lengths on Illumina's Hiseq platform. Reads were trimmed with Trimmomatic (Bolger et al., 2014). Mapping and quantification was performed from raw data using Bowtie2 (Langmead and Salzberg, 2012) and Express (Roberts et al., 2011) to the human genome (Hg38). From the 56,142 quantified RefSeq transcripts,

26,243 were removed due to low abundance (at least 1 count per million in less than 15% of samples). Two samples were removed from further analysis due to poor quality (low average counts). The dataset for analysis consisted of 29,881 log-transformed transcripts and 93 samples.

Univariate testing to quantify association between gene expression, primary group and relevant confounders was performed using generalized linear models and False Discovery Rate (FDR, Benjamini-Hochberg correction) corrected p values to control for multiple testing. We first considered differential expression gene expression explained by primary group controlling for age, sex and country. These analyses resulted in 322/2198 differentially expressed transcripts at the p < 0.01 and p < 0.05 level, after correcting for multiple testing. Second, we considered two more stringent designs, gene expression explained by primary group controlling for age, sex, geographical area and auto-antibody, then these in addition to viral load. The former resulted in 3 differentially expressed transcripts at the p < 0.05 level (5% FDR), namely, *RAB11FIP5*, *SYT11* and *RAP2A*. The latter resulted in a single significant transcript, *RAB11-FIP5*, with p < 0.0007 and 0.816-fold change.

The sample filtering, processing and statistical analysis were performed in R.

### Determination of RAB11FIP5 expression in immune cell subsets
Cryopreserved PBMCs from the individuals in the bnAb and control group were thawed and stained with fluorescently labeled antibodies for cell surface markers (BD) for multiparameter flow cytometry as previously described (Moody et al., 2016). CD8 T cells were defined as CD3+CD8+, B cells were defined as CD19+CD4-, CD4 T cells were defined as CD4+CD19-CD8- and non-B/T were CD19-CD4-CD8-. The non-B/T population was further subdivided into monocytes (CD14+), NK cells (CD56+CD16+CD3-CD14-), pDCs (CD14-CD19-CD3-CD16-CD56-HLA-DR+CD123+CD11c-) and mDCs (CD14-CD19-CD3-CD16-CD56-HLA-DR+CD123-CD11c+). Cell populations were sorted into RLTplus lysis buffer and total RNA was purified using RNeasy micro kit (QIAGEN).

For quantitative PCR, RNA was reverse transcribed using the High-Capacity RNA-to-cDNA kit (ThermoFisher) and qPCR was carried out in duplicate wells using the Taqman probe for *RAB11FIP5* transcript (Hs00392033_m1;ThermoFisher) and *GAPDH* (Hs03929097_g1;ThermoFisher). Expression of *GAPDH* was subtracted from *RAB11FIP5* to normalize for input and the resulting delta CT values were log transformed to calculate relative expression.

### RNA-seq of bulk NK cells
RNA from sorted NK cells was subjected to reverse transcription and amplification using the Smartseq ultra-low v4 kit (Takara Bio USA). 200pg of amplified cDNA was prepared for Illumina sequencing using the Nextera XT library preparation kit (Illumina). Libraries were quantified using qPCR (Kapa Biosystems) and sequenced to a minimum depth of 25 million reads per sample (2x75bp reads) on the Illumina NextSeq. After sequencing, fastq files were quality filtered and trimmed using TrimGalore (https://www.bioinformatics.babraham.ac.uk/projects/trim_galore/) and aligned to the human genome (Hg38) using STAR (Dobin et al., 2013). After reference alignment read counts on each gene were quantified by HTseq (Anders et al., 2015) and significantly differentially expressed transcripts were determined by DeSeq2 R package (Love et al., 2014). Biological pathway analysis was performed using Ingenuity Pathway Analysis (QIAGEN).

### Single-cell RNA sequencing of NK cell populations
Three NK cell subsets (all CD3-CD14-CD19-): CD56bright (CD56+CD16-), CD56dim (CD56dim, CD16+) and CD56neg (CD56-CD16+) populations from a single HIV-infected donor who developed bnAbs were sorted into PBS containing 0.04%BSA by flow cytometry. Cellular suspensions were loaded on a GemCode Single-Cell instrument (10X Genomics, Pleasanton, CA) to generate single-cell beads in emulsion (Zheng et al., 2017). Single-cell RNA-seq libraries were then prepared using a GemCode Single Cell 3′ Gel bead and library kit (10X Genomics). Single-cell barcoded cDNA libraries were quantified by quantitative PCR (Kappa Biosystems, Wilmington, MA) and sequenced on an Illumina NextSeq 500 (San Diego CA). Read lengths were 26 bp for read 1, 8 bp i7 index, and 98 bp read 2. Cells were sequenced to greater than 50,000 reads per cell. The Cell Ranger Single Cell Software Suite was used to perform sample de-multiplexing, barcode processing and single-cell 3′ gene counting (Zheng et al., 2017). Reads were aligned to human genome release Hg38 (Dobin et al., 2013; Zheng et al., 2017). Graph based cell clustering, dimensionality reduction and data visualization were analyzed by the Seurat R package (Satija et al., 2015). Cells that exhibited high transcript counts, > 0.1% mitochondrial transcripts were excluded from analysis. During subset aggregation libraries were normalized by mapped read depths. Differentially expressed transcripts were determined in the Seurat R package utilizing the Likelihood-ratio test for single cell gene expression statistical test (McDavid et al., 2013). Graphics were generated using the Seurat and ggplot2 R packages.

### Phenotypic and functional analysis of PBMC NK cell subsets
The following fluorochrome-conjugated antibodies were utilized for identification and phenotypic analysis of NK cell subsets: CD14 BV510, CD19 BV510, CD56 PE Dazzle, CD3 BV650, CD16 PERCP or CD16 BV711, PD1 BV711, Streptavidin- BV711, Siglec-7 PE, CD85j biotin (Biolegend), CD4 APC-eFluor 780, CD8 Alexa700 (eBioscience), NKG2A Pe-Cy7, KIR2DL2/L3/S2 APC [CD158b1/b2.j] (Beckman Coulter), NKG2C PE, KIR2DL1/2DS5 APC IgG1 [CD158a], KIR3DL2 APC (R&D systems), CD57 BV605, (BD Biosciences), KIR3DL1 APC [CD158e1] (Miltenyi), for surface antigens; Granzyme B FITC, Perforin PE (Biolegend), IFN-γ BV421 (BD Biosciences), TNF-α BV711 (Biolegend), FcεRI-γ FITC (Millipore) for intracellular staining; and PLZF APC (BD Biosciences) for intranuclear staining.

For phenotypic analysis of NK cells, cryopreserved PBMC from HIV-1 infected subjects and seronegative donors were washed in PBS and surface stained at 4°C for 20 min with saturating concentrations of different combinations of antibodies in the presence of fixable live/dead stain (Invitrogen). Cells were fixed and permeabilized for the detection of intracellular antigens. For the detection of intranuclear markers the Foxp3 intranuclear staining buffer kit (eBioscience) was used according to the manufacturer's instructions.

For analysis of NK cell functionality, PBMC were incubated with the 721.221 MHC class I low cell line (5:1 E:T ratio) for 6 hours at 37°C to stimulate NK cell activation in the presence of CD107a APC-H7 antibody (BD Biosciences, Cowley, UK). GolgiStop (containing Monensin, 1/1500 concentration, BD Biosciences) and GolgiPlug (containing brefeldin A, 1/1000 final concentration, BD Biosciences) were added for the last 5 hours of culture. Following incubation cells were washed and stained for extracellular receptors as described above prior to permeabilization and intracellular staining for TNF-$\alpha$ and IFN-$\gamma$.

All samples were acquired on a BD Fortessa X20 using BD FACSDiva8.0 (BD Bioscience) and data were analyzed using FlowJo 9 (TreeStar). Stochastic neighbor embedding (SNE) analysis was performed using the mrc.cytobank platform. The FCS file concatenation tool was used to concatenate multiple FCS files into a single FCS file prior to uploading to cytobank.

### *In vitro* co-culture system to assess the ability of NK cells to reduce CD4 Tfh availability and B cell responses

Mononuclear cells were isolated from leukapheresis samples from healthy, HIV-seronegative donors (obtained from the NHS Blood and Transplant Service) by Histopaque density gradient centrifugation (Sigma). Untouched NK cells were separated by negative selection using a NK cell isolation kit (Miltenyi). CD4 T cells were enriched by negative selection using a CD4 T cell isolation kit (Miltenyi), then CD4 Tfh cells were sorted from this population as live CD3+CD4+CD127hiCD25loCXCR5+ cells (to exclude regulatory T cells from the co-culture). Cell sorting was performed using an Aria III Instrument (BD Biosciences). The NK cells were stimulated with 100 IU/ml IL-2 (Proleukin; Novartis) + 10ng/ml IL-12-p70 (PeproTech) + 20ng/ml IL-15 (Miltenyi) + 100ng/ml IL-18 (MBL) for 48h. The CD4 Tfh cells were labeled with 1 uM Cell Trace Violet (Life Technologies) following the manufacturer's instructions and were stimulated with 1ug/ml Staphylococcal Enterotoxin B (SEB) + 20 IU/ml IL-2 for 48h. NK cells and Tfh cells were stimulated separately at a concentration of $1 \times 10^6$ cells/ml in RPMI 1640 (Life Technologies) containing 10% heat-inactivated fetal bovine serum (Sigma), 1% penicillin-streptomycin (Sigma), 1% sodium pyruvate (Sigma), 1% Glutamax (Life Technologies), 1% non-essential amino acids (Life Technologies) and 2 mM beta-mercaptoethanol (Life Technologies) incubated at 37°C in 5% $CO_2$. After initial activation, CD4 Tfh cells and NK cells were washed and CD4 Tfh cells were cultured at $30 \times 10^3$ cells/well in the presence of 1ug/ml SEB either with or without $15 \times 10^4$ NK cells for 18h. Untouched CD27-CD19+ naive B cells were isolated from the same donors using the naive B cell isolation kit II from Miltenyi. $60 \times 10^3$ total naive B cells were then added to the NK-Tfh co-culture wells to give a final ratio of 2:1:5 (B:Tfh:NK). Co-cultures were performed in U-bottomed 96-well plates with a final volume of 200 ul. After 6 days of B:Tfh:NK co-culture, supernatants were collected and cells were incubated with Human TruStain FcX (FC receptor blocking solution; Biolegend) for 10min and then stained with an antibody cocktail including anti-CD3 PE-Texas Red (S4.1, Life Technologies), anti-CD4 PE (SK3, BD Biosciences), anti-CD19 BV650 (HIB19, Biolegend), anti-CD20 Pecy5 (2H7, Biolegend), anti-CD27 BV711 (clone O323, Biolegend), anti-CD38 BV785 (HIT2, Biolegend), anti-CD56 BV605 (NCAM16.2, BD Biosciences), anti-IgD PEcy7 (clone IA6-2, Biolegend), anti-IgM Alexa Fluor (AF)647 (clone MHM-88, Biolegend), and Live Dead Near Red for viability (Life Technologies) for 15 min at room temperature, fixed with 2% paraformaldehyde (Santa Cruz) for 10 min, and analyzed by flow cytometry. Before acquisition, Countbright absolute counting beads (Life Technologies) were added to quantify cells. Flow cytometry was performed on a LSR Fortessa instrument (BD Biosciences) and data were analyzed with FlowJo version 9 software (Tree Star). Class-switched memory B cells were identified as live CD3-CD4-CD56-CD19+IgD-IgM-CD20+CD38+/− cells and plasmablasts as live CD3-CD4-CD56-CD19+IgD-IgM-CD20-CD38+ cells. Antibody production was assessed by measuring supernatant levels of total IgM and IgG using human IgM and IgG development kits (ALP; Mabtech).

### NK-92 cell culture

The NK-92 human cell line (ATCC CRL-2407) was cultured in Alpha Minimum Essential medium (GIBCO, Catlog#12561072) supplemented with 2 mM L-glutamine, 0.2 mM inositol, 0.1 mM 2-mercaptoethanol, 0.02 mM folic acid, 200 U/ml recombinant IL-2 (PeproTech, Catlog#200-02), 12.5% horse serum (GIBCO, Catlog#16050122) and 12.5% fetal bovine serum (GIBCO, Catlog#10099141).

### Generation of a Rab11Fip5 stably expressing NK-92 cell line

The human *RAB11FIP5* gene was synthesized (Genscript), cloned into lentiviral vector pLVX-IRES-ZsGreen1 (Clontech,Catalog#632187), and co-transfected into 293FT cells with lentiviral packaging plasmids pMD2.G (Addgene plasmid #12259) and psPAX2 (Addgene plasmid #12260). Lentivirus particles were harvested 48-72h post-transfection and inoculated onto NK-92 cells. Four days after lentiviral infection, the Rab11Fip5 positive NK-92 cells were sorted by FACS (BD FACSAria II) based on zsGreen fluorescent protein expression. NK-92 cells transduced with lentiviral empty vector (zsGreen only) served as a control cell line. The stable cell lines were validated by western blot using a Rabbit anti-human Rab11Fip5 polyclonal antibody (Sigma, Catlog#HPA036407). For western blot, cells were treated with RIPA lysis and Extraction Buffer (Thermo Scientific) on ice for 10 minutes, sonicated, and subjected to NuPAGE 4%–12% Bis-Tris Protein Gels (Thermo Scientific). After transfer to PVDF membrane (Invitrogen) The blots were blocked with Bløk - CH Noise Cancelling Reagents (Millipore, Catalog# WBAVDCH01) for 1 hour, and probed with Rab11Fip5 (Sigma, Catlog#HPA036407) and GAPDH (Invitrogen, Catalog# MA5-15738) primary antibodies for 2 hours, followed by incubation for 1 hour with the corresponding horseradish peroxidase (HRP)-conjugated secondary antibodies.

### Analysis of degranulation and cytokine production of RAB11FIP5-transduced NK-92 cells

For intracellular staining and degranulation assay, NK-92/Rab11Fip5 cells and NK-92/vector control cells were stimulated with 500 ng/ml PMA and 5 ug/ml ionomycin in the presence of BV711 anti-human CD107a antibody (5 ug/ml; Biolegend, Catalog# 328640) and GolgiStop protein transport inhibitor (BD, Catalog#554724) for 2 hours. Cells were then stained with Aqua viability dye (Thermo Fisher, Catalog#L34957), fixed with 2% PMA, and stained with PE/Cy7 anti-human TNF-α Antibody (Biolegend, Catalog# 328640) and Alexa Fluor 647 anti-human IFN-γ Antibody (Biolegend, Catalog# 502516) in Permeabilization Buffer (Invitrogen, Catalog# 88-8824). Data were collected by the High-throughput Sampler (HTS) in BD LSR II flow cytometer and analyzed with FlowJo software.

For analysis of cytokine secretion, cells were PMA/ionomycin stimulated for 2 hours in the absence of GolgiStop and the CD107a antibody, the supernatants were harvested and cytokine levels analyzed by Luminex using a 17-plex Magnetic Bead Panel (Millipore), following the manufacturer's instructions.

### Granzyme B-based cytotoxicity assays

For the granzyme B (GzB)-based cytotoxicity assay (Pollara et al., 2011), the K562 cell line was used as a NK-stimulatory target, while the CEM.NKRCCR5 cell line was used as negative control. Target cells were counted, washed, resuspended in RPMI containing 10% FBS at $1 \times 10^6$ cell/ml, and labeled with a fluorescent target-cell marker (TFL4; OncoImmunin, Inc., Gaithersburg, MD) and a viability marker (NFL1; OncoImmunin, Inc.) for 15 minutes in at 37°C. After washing twice in media, viable cells were counted using a Muse Cell Analyzer (MilliporeSigma) and mixed with NK-92 effector cells at final viable effector to viable target (E:T) ratio of 60:1, 20:1, 6:1 and 2:1 in a 96-well V-bottom plate. GzB substrate (OncoImmunin, Inc.) was then added into the cell mixture. After incubating for 15 minutes at RT, the plates were subsequently centrifuged for 1 minute at 300 × g and incubated for 1 hour at 37°C in 5% CO2. After two washes with washing buffer (PBS+1% FBS), cells were resuspended in 225 μL of washing buffer, and acquired directly from the assay plate within 6 hours using a HTS on a LSRII (BD Bioscience). The signal for each fluorophore was detected using: 1) a 640nm/40mW laser and 660/20 filter for TFL4 2) a 405nm/50mW laser and 450/50 filter for NFL1; 3) a 488nm/20mW laser and the combination of 505LP with 525/50 filters for the GzB substrate. Data analysis was performed using FlowJo software, and the results are expressed as %GzB activity, defined as the percentage of viable target cells positive for proteolytically active GzB (i.e., cells recognized by the effectors) out of the total viable target cell population. Area under the curve (AUC) values were calculated and shown for each independent repeat.

### QUANTIFICATION AND STATISTICAL ANALYSIS

The NK cell surface marker and functional phenotyping was analyzed using linear regression. Because the measures are proportions, the outcome was first arcsine transformed as a variance stabilizing measure. The models all included group as a predictor and the geometric mean viral load of the participant as a covariate. The inclusion of viral load as a covariate entails that the effect was present and significant independent of viral load. All of the p values from the analysis were combined and the Benjamini-Hochberg false discovery rate correction was applied and those are the p values reported. Other univariate comparisons were tested for significance using the Wilcoxon-Mann-Whitney with FDR correction unless otherwise specified. All of these analyses were performed using SAS v9.4 (SAS Institute, Inc.).

For data analysis of marker co-expression data, Prism 7 (GraphPad Software) was used. Student's t test was used for single comparisons of independent groups in SPICE. Permutation tests were performed in SPICE version 5.35.

For the bulk NK cell RNA-seq, significantly differentially expressed transcripts were determined by DeSeq2 R package (Love et al., 2014). Biological pathway analysis was performed using Ingenuity Pathway Analysis (QIAGEN). For single-cell RNA-seq, differentially expressed transcripts were determined in the Seurat R package utilizing the Likelihood-ratio test for single cell gene expression statistical test (McDavid et al., 2013). Graphics were generated using the Seurat and ggplot2 R packages.

For all other univariate comparisons, the Wilcoxon-Mann-Whitney with FDR correction unless otherwise specified calculated using SAS v9.4 (SAS Institute, Inc.).

Exact number of subjects/replicates indicated in results and figure legends along with the precise statistical measures utilized.

### DATA AND SOFTWARE AVAILABILITY

The accession number for the bulk RNA-seq data reported in this paper is GEO: GSE115449. The accession number for the single-cell RNA-seq data reported in this paper is SRA: SRP150325. Any additional analysis files are available upon request from the authors.
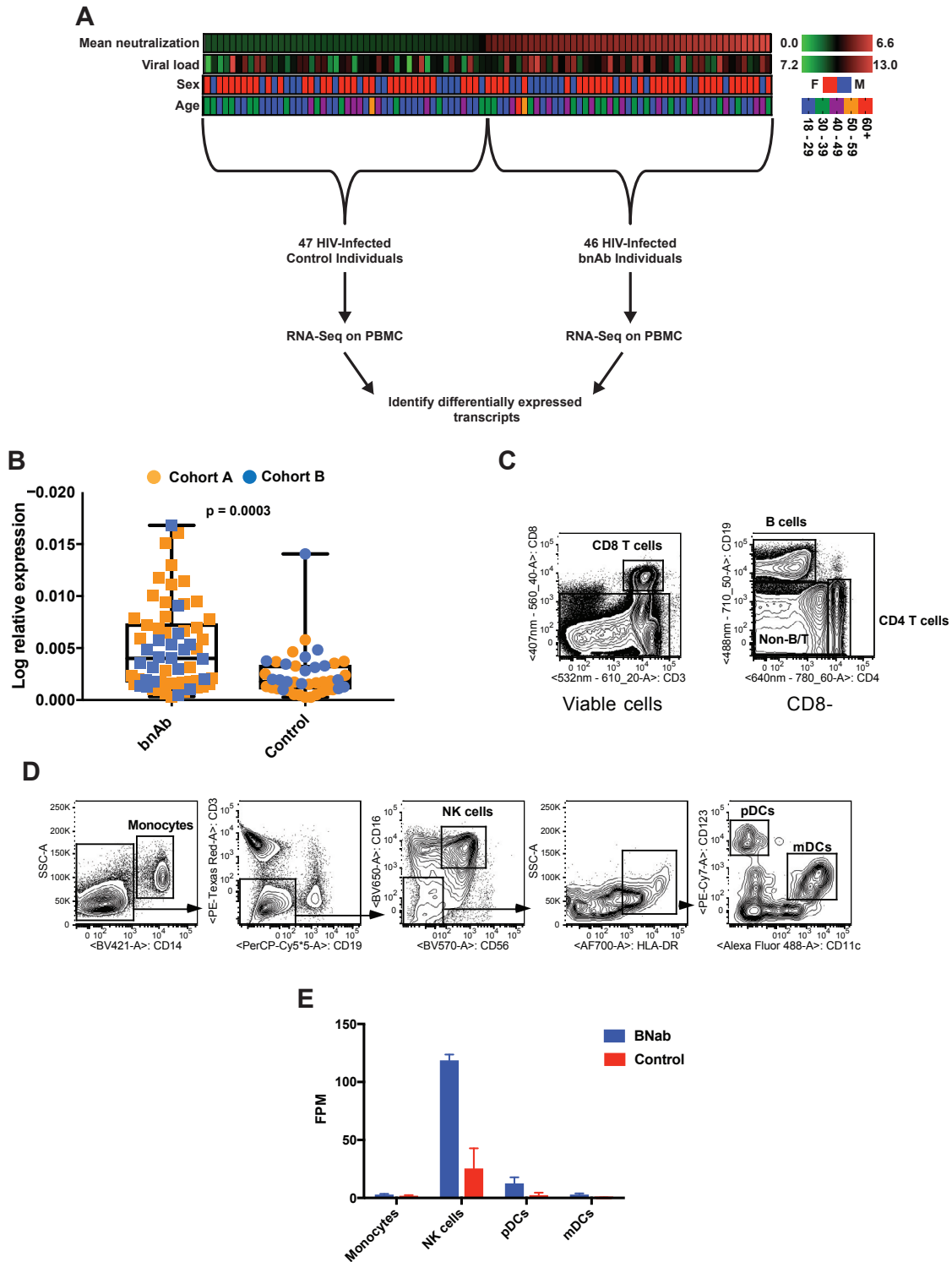
**Figure S1. *RAB11FIP5* Is Significantly Upregulated in Individuals Who Develop bnAbs, Related to Figure 1**

(A) Heatmaps of metadata from the cohort of individuals studied. Natural log of geometric mean (ID50) neutralization and mean viral load from sampled time points in addition to sex and age. Age and sex did not differ significantly between the bnAb and control groups. A more detailed description of these subjects and attributes of the larger cohort from which they were selected are provided in Moody et al. (2016).

*(legend continued on next page)*

(B) Quantitative PCR for *RAB11FIP5* expression from RNA isolated from individuals' PBMCs. Cohort A bnAb n = 41; Cohort A control n = 25; Cohort B bnAb n = 21; Cohort B control n = 16. *P value* determined by Wilcoxon-Mann-Whitney. No statistically significant difference between the bnAb and Control group was detected for Cohort B samples alone.

(C and D) Representative flow cytometry density plots demonstrating the populations sorted for quantitative PCR and RNA-seq.

(E) *RAB11FIP5* expression level measured by RNA-seq in immune subsets, the fraction of reads per million of mapped reads (FPM) graphed with SEM.
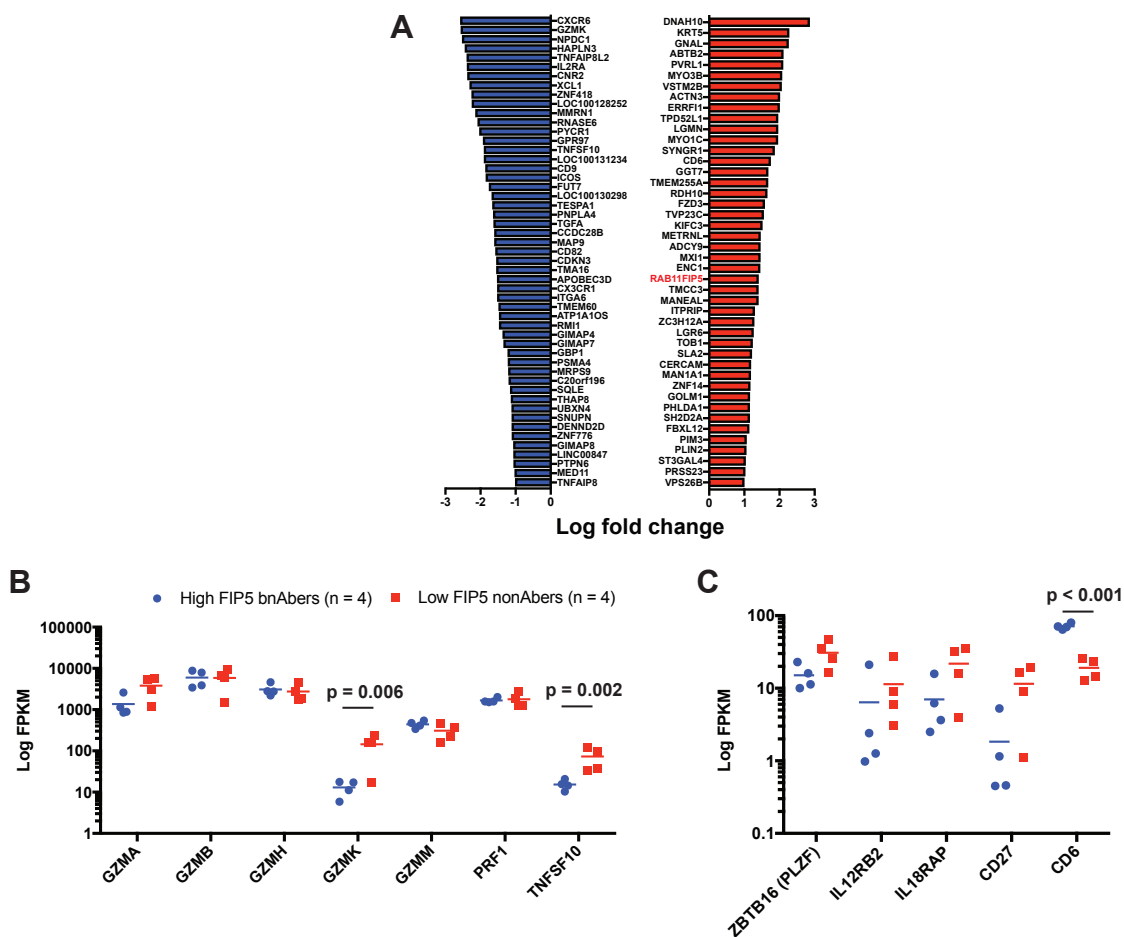
**Figure S2. Transcriptome Sequencing of NK Cells from bnAb and Control Individuals, Related to Figure 1**

(A) Bar graph of log fold-change of genes downregulated (blue) or upregulated (red) in bnAb subject NK cells (n = 4) compared with control subject NK cells (n = 4) determined by RNA-seq.

(B and C) Dot plots of log fragments per kilobase of transcript per million mapped reads for genes in NK cells from bnAb (red) and control groups (blue). Line indicates group mean. Adjusted P values generated by DeSeq2. Values not corrected for viral load.
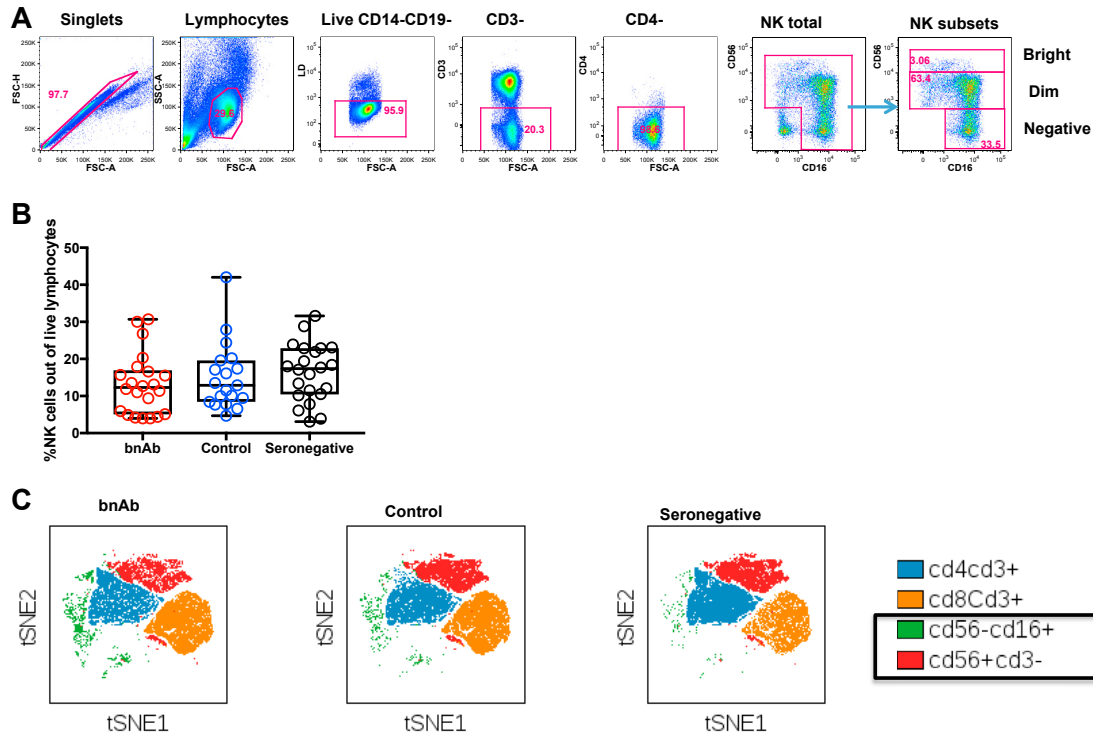
**A**

Singlets | Lymphocytes | Live CD14-CD19- | CD3- | CD4- | NK total | NK subsets

Bright
Dim
Negative

**B**



**C**

bnAb | Control | Seronegative

cd4cd3+
cd8Cd3+
cd56-cd16+
cd56+cd3-

**Figure S3. NK Cell Gating Strategy and NK Cell Frequency, Related to Figure 2**

(A) Representative example gated on live CD14-CD19-CD3-CD4- lymphocytes; CD56 and CD16 are used to identify NK cells, discriminating between populations on the basis of CD56bright, dim and negative expression levels.

(B) Boxplots of the percentage of NK cells out of live lymphocytes in individuals in the bnAb (red; n = 22), control (blue; n = 19) and HIV-seronegative (black; n = 22) groups. Each symbol represents data from an individual subject and the box-and-whisker plots show the median, quartiles and range.

(C) ViSNE map of NK and T cell distribution based on CD3, CD4, CD8, CD56 and CD16 expression from compiled subjects in the bnAb, control and HIV seronegative group. CD4CD3+ T cells are shown in blue, CD8CD3+ T cells in orange, CD56+CD3- NK cells in red and the CD56-CD16+ NK cell subset in green.
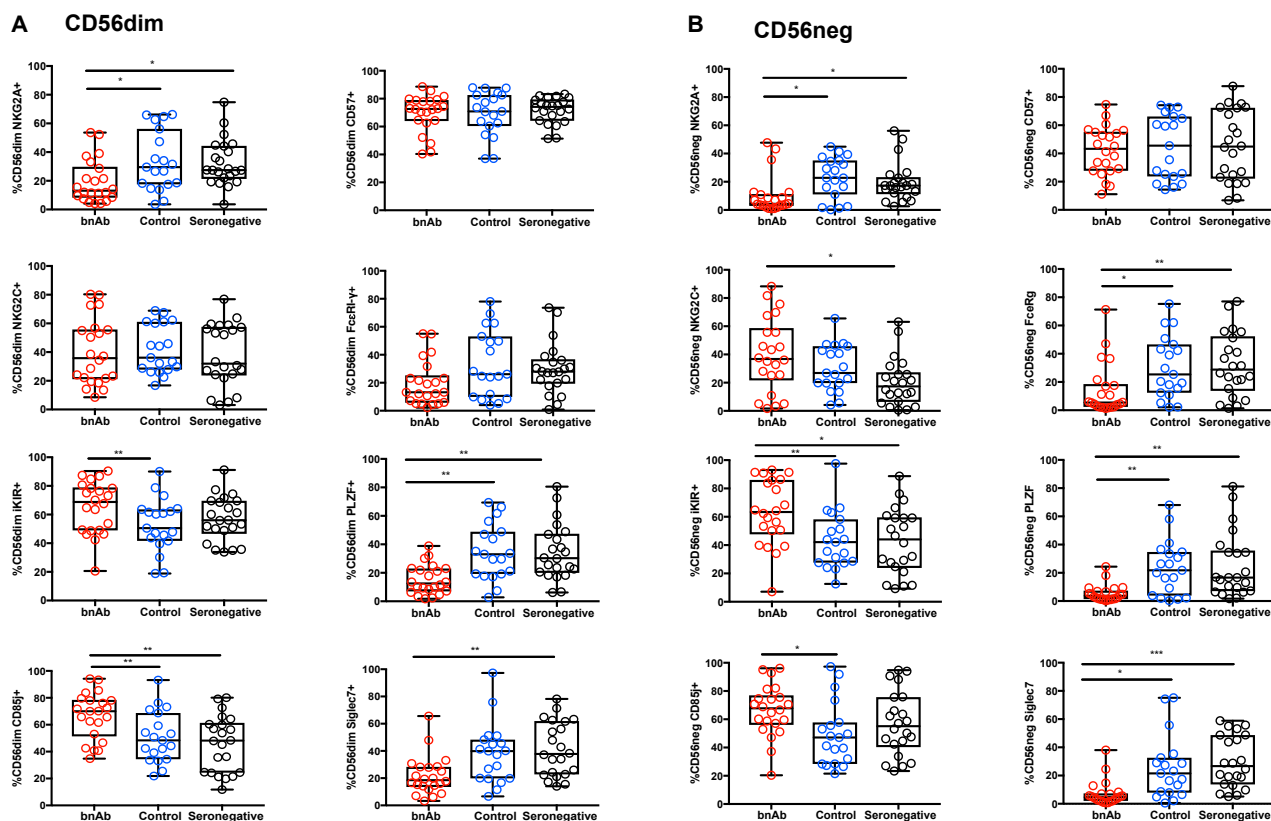
**Figure S4. CD56dim and CD56neg Subset Phenotypic Analysis, Related to Figure 3**

(A and B) Summary boxplots of expression of NKG2A, NKG2C, iKIR (cocktail of antibodies against KIR2DL1/S5, KIR2DL2/L3/S2, KIR3DL2, KIR3DL1), CD85j, CD57, FcεRI-γ, PLZF and Siglec7 on CD56dim NK cells and (B) on the CD56neg NK cell subset in bnAb (red; n = 22), control (blue; n = 19) and HIV seronegative individuals (black; n = 22). Each symbol represents data from an individual subject and the box-and-whisker plots show the median, quartiles and range. *p < 0.05, **p < 0.01, ***p < 0.001. P values corrected for MCA and viral load.
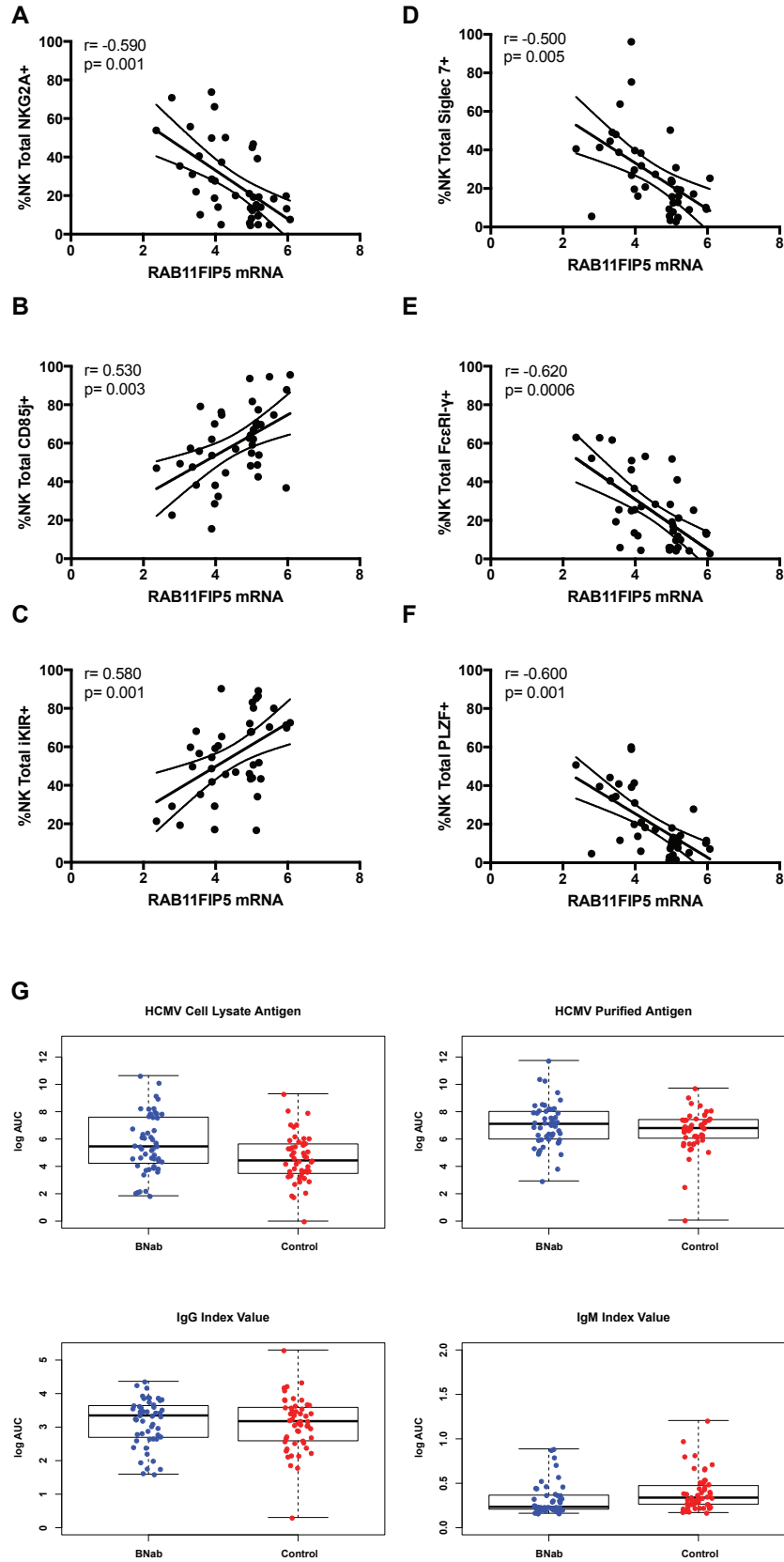
**A** r= -0.590 p= 0.001

**B** r= 0.530 p= 0.003

**C** r= 0.580 p= 0.001

**D** r= -0.500 p= 0.005

**E** r= -0.620 p= 0.0006

**F** r= -0.600 p= 0.001

**G**

HCMV Cell Lysate Antigen

HCMV Purified Antigen

IgG Index Value

IgM Index Value

*(legend on next page)*

**Figure S5. *RAB11FIP5* Transcript in Total PBMC Correlates with Receptor Expression on Total NK Cells, Related to Figure 3**

(A–F) Spearman correlation of *RAB11FIP5* mRNA levels in total PBMC with total NK cells expression of (A) NKG2A, (B) CD85j, (C) iKIR (cocktail of antibodies against KIR2DL1/S5, KIR2DL2/L3/S2, KIR3DL2, KIR3DL1), (D) Siglec 7, (E) Fc$\varepsilon$RI-$\gamma$, and (F) PLZF. *p < 0.05, **p < 0.01, ***p < 0.001. P values corrected for MCA. (G) Plasma antibody binding to HCMV cell lysate antigen or recombinant HCMV gB antigen measured by ELISA and Bio-Rad clinical CMV assay for individuals in the bnAb (blue) and control group (red). Values displayed as log area under the curve. Cutoff for positivity for the IgG and IgM clinical assay was > 1.1.
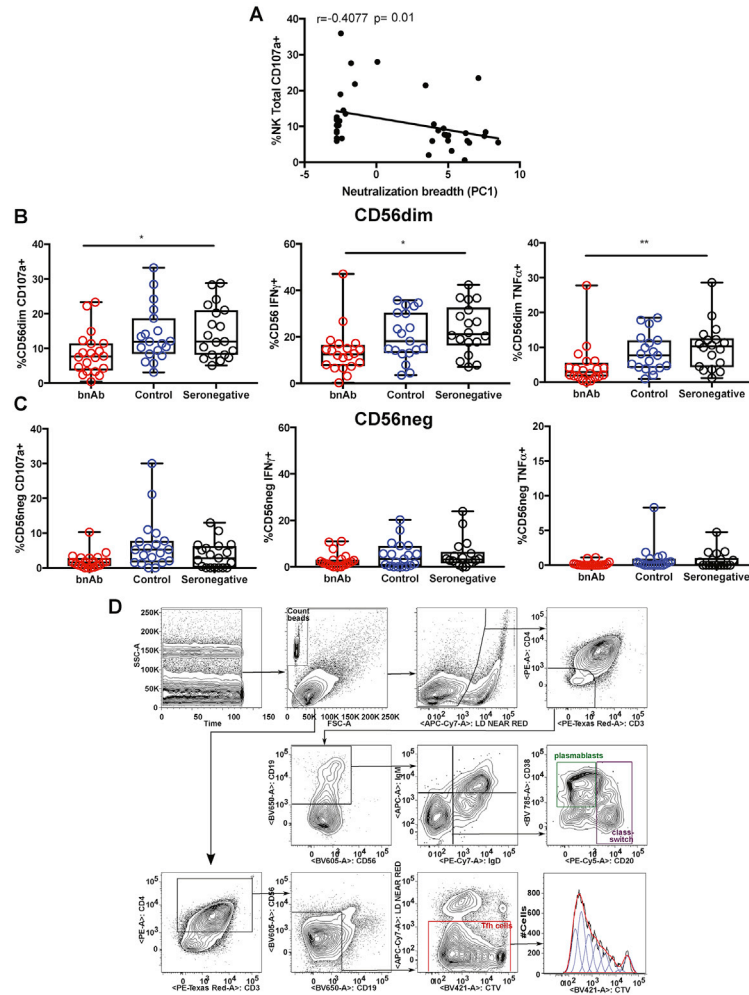
**Figure S6. Functional Analysis of CD56dim and CD56neg NK Subsets and Gating Strategy for Analysis of NK:Tfh:B Cell Co-culture, Related to Figures 4 and 5**

(A) Spearman correlation of percentage of total NK cells undergoing degranulation (assessed by CD107a expression) on exposure to target cells with plasma HIV-1 neutralization breadth (PC1).

(B and C) Summary boxplots for CD107a expression, IFN-γ and TNF-α production from (B) CD56dim NK cells and (C) CD56neg NK cells following target cell stimulation in bnAb (red), control (blue) and HIV seronegative individuals (black). Each symbol represents data from an individual subject and the box-and-whisker plots show the median, quartiles and range. *p < 0.05, **p < 0.01. P values corrected for MCA and viral load.

(D) Class-switched memory B cells were identified as live CD3-CD4-CD56-CD19+IgD-IgM-CD20+CD38+/− cells and plasmablasts as live CD3-CD4-CD56-CD19+IgD-IgM-CD20-CD38+ cells. Tfh cells were identified as live CD3+CD4+CD19-CD56- cells. The division index was calculated using Flowjo software. CountBright absolute counting beads were used to calculate absolute numbers. The staining shown is from a representative subject (Tfh+B cell only condition).
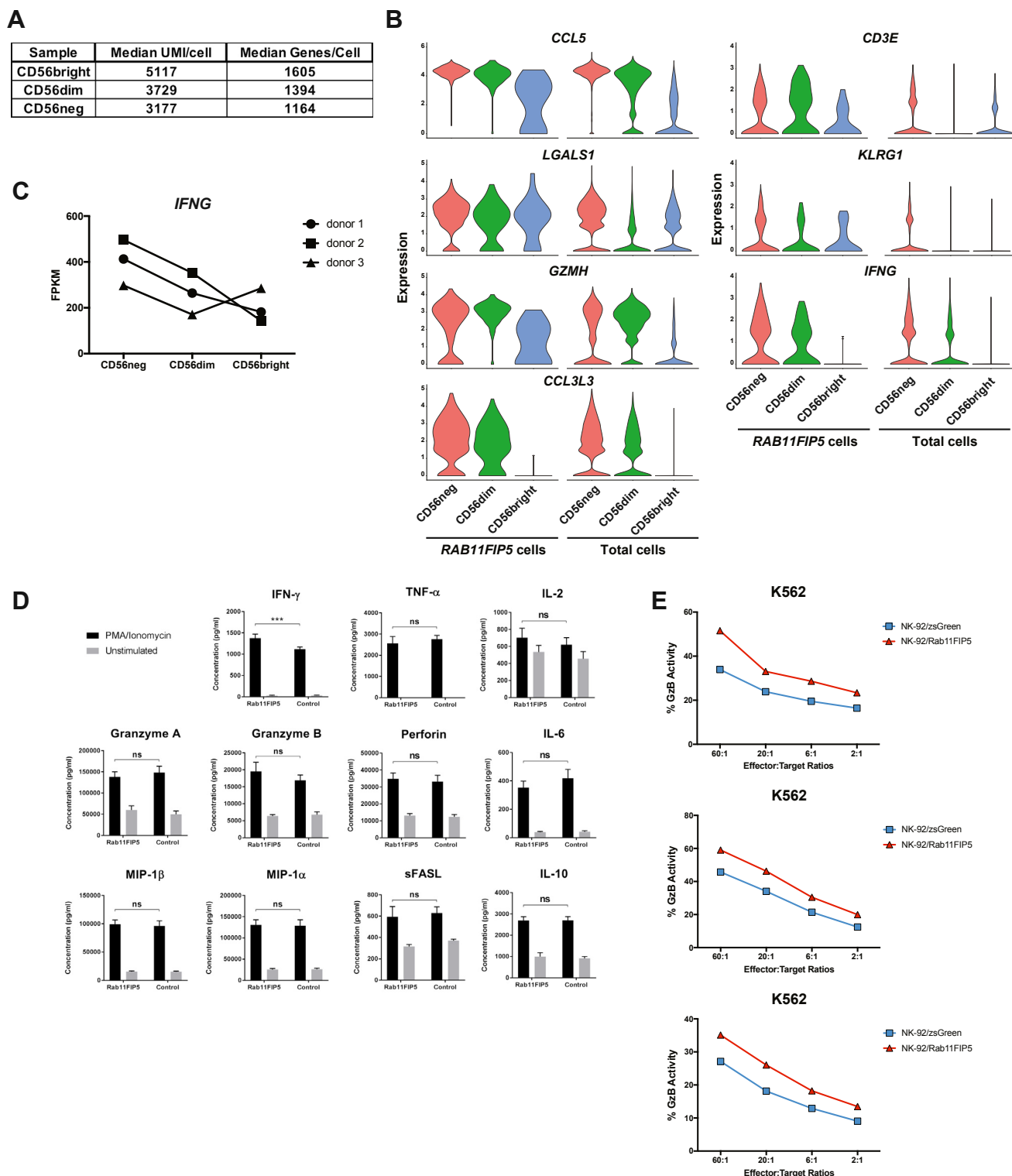
Cell



**Figure S7. Transcript Expression from Bulk NK Cell RNA-Seq and Cytokine Secretion from Rab11Fip5-Expressing NK-92 Cells Measured by Luminex Assay Together with Analysis of Their Cytolytic Activity, Related to Figures 6 and 7**

(A) Median unique molecular identifiers (UMIs) and genes detected per cell in the scRNA-seq datasets.

(B) Single-cell RNA-seq analysis was performed on CD56bright, dim and neg NK subsets isolated from a single donor by cell sorting. Violin plots of transcripts significantly upregulated in *RAB11FIP5*-expressing cells (red) compared to cells not expressing *RAB11FIP5* (blue). Data for each NK cell subset is shown separately for significant genes (determined by likelihood ratio test and p ≤ 0.05). Normalized transcript expression is shown on the y axis.

*(legend continued on next page)*

(C) NK cells from three HIV-infected donors were sorted into subsets on the basis of CD56 expression and subjected to bulk RNA-seq. Reads were aligned to the human genome (Hg38) and Fragments Per Kilobases of transcript per Million mapped reads (FPKM) were determined for each donor in each subset for *IFNG* transcript expression.

(D) NK-92/*RAB11FIP5* transduced cells and NK-92/empty vector control cells were stimulated with 500 ng/ml PMA and 5 μg/ml ionomycin for 2 hours. Supernatants were harvested and levels of GM-CSF, sCD137, IFN-γ, sFas, sFasL, Granzyme A, Granzyme B, IL-2, IL-4, IL-5, IL-6, IL-10, IL-13, MIP-1α, MIP-1β, TNF-α and perforin were analyzed by Luminex assay. All the cytokines in range of the standard curves are shown. Error bars represent standard deviation of quadruplicate wells. Wilcoxon-Mann-Whitney was utilized for statistical analysis. ns, not significant; ***$p \leq 0.001$.

(E) Granzyme B (GzB)-based cytotoxicity assays performed using NK-92/*RAB11FIP5* (red) or NK-92/ZsGreen control (blue) cells as effectors and K562 cells as targets at different effector:target ratios. The percentage of cells positive for proteolytically active GzB is represented as % GzB activity. Data from 3 individual experiments, each of which was were performed in triplicate, are shown.